Elsevier Editorial System(tm) for Journal of Hydrology
Manuscript Draft

Manuscript Number: HYDROL10488R2

Title: WEATHERING OF PLAGIOCLASE ACROSS VARIABLE FLOW AND SOLUTE TRANSPORT REGIMES

Article Type: Research Paper

Keywords: gravity flow fracture; capillary flow microfracture; advective transport; diffusive transport; open system; semi-open system; weathering; plagioclase; hydraulic diffusivity

Corresponding Author: Dr. Fernando A.L. Pacheco,

Corresponding Author's Institution: Trás-os-Montes e Alto Douro Univ.

First Author: Fernando A.L. Pacheco

Order of Authors: Fernando A.L. Pacheco; Cornelis H Van der Weijden, Prof.

Cover Letter

Fernando A.L. Pacheco
Department of Geology and Centre for Chemistry
Trás-os-Montes and Alto Douro University
5000 Vila Real
Portugal

Professor Laurent Charlet
Editor
Journal of Hydrology

November 7, 2011

HYDROL10488R1: Editor decision - revise (minor revision)

Dear Prof. Charlet,

We are very pleased with your decision regarding our manuscript. We addressed the very minor corrections pointed out by reviewer #1, related to incorrect citations to borehole numbers, as can be consulted in the DOC file *Revision_Notes*. The revised version of the manuscript is given in the DOC file *Revision_Changes_Marked* (an annotated manuscript showing the very minor changes relative to the original manuscript (HYDROL10488R1), affecting just three lines of that ms. The final version of the manuscript is given in the DOC file *Manuscript_Final*. Tables and corresponding legends are provided as a separate DOC file, the same happening with the figure captions. Figures as provided as TIFF format images, with resolution 600 or 1200 DPI.

We hope you are satisfied with the revised version, and that the paper can be published soon.

Kind regards,
Fernando A.L. Pacheco

Revision Notes
Click here to download Revision Notes: Revision_Notes.doc

Revision Notes

Reviewer #1

Correct the "Nr" in text.
The reviewer is right

Line178: Nr23 ? Nr22
Changed Nr 23 to Nr 22

Line183 and Line192: Nr4, 18, and 19 ? Nr4, 19 and 20 (?)
Changed Nr 4, 18 and 19 to Nr 4, 19 and 20

Line402: Nr10, 11, 16 and 25 ? Nr11, 12, 17 and 26
Changed Nr 10, 11, 16 and 25 to Nr 11, 12, 17 and 26

RESEARCH HIGHLIGHTS

Weathering studies based on the microsystem concept were initiated by Korzhinskii (1959), and recently developed by Meunier et al. (2007). Basically, these studies associate precipitation of specific secondary products (e.g. smectite, halloysite) to specific locations in a fractured rock mass (e.g. capillary flow micro fractures, gravity-flow fractures) where specific flow and transport regimes prevail (e.g. chemical diffusion, advection). The scale of these studies was the thin section scale. The first research highlight of this paper is the extrapolation of the weathering analysis based on the microsystem concept to the macroscopic scale, applying it to fault zones underlying a soil plus saprolite cover.

White and Brantley (2003) showed that factor time explains the discrepancy reported in many studies between weathering rates estimated in the field and in the laboratory. The field weathering rates reported in that study were mostly solid-state weathering rates based on the differences between elemental, isotopic and mineral compositions measured in present-day regoliths and in the assumed protolith. In these cases, variable time (t) represents the entire time span of a weathering episode, commonly on the order of thousands to million years. These rates are not directly reconcilable with solute-flux rates, also estimated in field studies, that stand for contemporary weathering during groundwater percolation in the fractured rocks, in which case t (travel time) is just a portion of that time window, frequently ranging from years to decades. The second highlight of this paper is a demonstration that reconciliation between solid-state and solute-flux weathering rates can be accomplished if the change in aquifer properties (hydraulic diffusivity, which is a proportion of the ratio between hydraulic conductivity and effective porosity) over the geologic times is accounted for in the weathering models.

References

Korzhinskii, D.S. (1959). *Physicochemical Basis of the Analysis of the Paragenesis of Minerals* (translation). Consultant Bureau, New York, 143 pp.

Meunier, A., Sardini, P., Robinet, J.C., Prêt, D. (2007). The petrography of weathering processes: facts and outlooks. *Clay Miner.*, 42: 415–435.

White, A.F., Brantley, S.L. (2003). The effect of time on the weathering of silicate minerals: why do weathering rates differ in the laboratory and field? *Chem. Geol.*, 202: 479–506.

WEATHERING OF PLAGIOCLASE ACROSS VARIABLE FLOW AND SOLUTE TRANSPORT REGIMES

Fernando A. L. Pacheco,[a]
Department of Geology & Centre for Chemistry,
Trás-os-Montes and Alto Douro University, Ap 1013, 5000 Vila Real
Portugal

Cornelis H. Van der Weijden,[b]
Department of Earth Sciences—Geochemistry, Faculty of Geosciences,
Utrecht University, P.O. Box 80.021 3508 TA Utrecht,
The Netherlands

Key-words: gravity flow fracture, capillary flow microfracture, advective transport, diffusive transport, open system, semi-open system, weathering, plagioclase, hydraulic diffusivity.

[a] Corresponding author, e-mail FPACHECO@UTAD.PT, Fax. +351 259 350480
[b] e-mail CHVDW@GEO.UU.NL, Fax +31 30 2535302

Abstract

The study area is situated in a fault zone with fractured granites and metassediments. In a conceptual model, infiltrating water first passes the bedrock cover of soil and saprolite and then partly enters the fractures. Weathering reactions of minerals occur in small pores and fissures in the bedrock cover zone to continue in the larger fractures. Pumping tests were carried out in a number of boreholes to measure the drawdown as a function of pumping time. From the results, values of transmissivity (T) could be derived. In combination with the storage coefficient (S) for similar fault zones, the hydraulic diffusivity ($D = T/S$) could be computed.

Water samples, collected from the boreholes, represent fluid packets with a history of weathering reactions in the bedrock cover and in the larger fractures. The major element composition of these samples was used by means of the SiB mass balance algorithm (Pacheco and Van der Weijden, 1996) to calculate the moles·L^{-1} of dissolved plagioclase (oligoclase with An ≈ 0.20) and the moles·L^{-1} of secondary phases (gibbsite, halloysite, smectite) precipitated along the flow paths of the samples. These results were then used to calculate the net dissolved silica concentrations ($[H_4SiO_4^0]$) related to dissolution of plagioclase followed by precipitation of each of the secondary phases. An interpretation of a plot of each of these $[H_4SiO_4^0]$'s versus D is that at $D < 0.7$ m^2·s^{-1}, dissolution of plagioclase is followed by precipitation of halloysite in the large fractures of the fault zone (open system), whereas at $D \geq 0.7$ m^2·s^{-1} precipitation of both halloysite and smectite occurs in the rock matrix with small fissures and pores (semi-open system). Before being pumped, the percolating fluids travelled 0.01 to 13.7 years. During these periods, plagioclase weathered at rates (W_{Pl}) of $10^{-(12.9\pm1.1)}$ moles·m^{-2}·s^{-1}, which are approximately 2.2 orders of magnitude higher than solid-state weathering rates reported in various field studies. In this study, it is

43 suggested that part of the apparent discrepancy between the results is due to changes in
44 hydraulic diffusivity of the weathering environments occurring over the geologic times.
45
46

47 *1. Introduction*

48

49 Weathering of rock forming minerals can be investigated in terms of microsystems, a concept
50 introduced by Korzhinskii (1959). These systems are located at each water–mineral contact
51 and are composed of the primary and secondary minerals and local solutions. They belong to
52 three categories: closed, semi-open and completely open (Meunier et al., 2007). In crystalline
53 rocks, closed microsystems are located at primary porosity and microfracture dead ends,
54 semi-open at microfractures and completely open at small fractures.
55 Groundwater flow and solute transport regimes within a microsystem depend on their
56 category: in a closed system, fluids are stagnant and therefore solute transport is limited; in a
57 semi-open system, water moves by capillarity and solute transport occurs by chemical
58 diffusion; and finally, in an open system, groundwater flow is controlled by gravity and
59 solute transport occurs by advection. The prevailing regimes determine the secondary
60 products derived from alteration of the parent minerals (Baynes and Dearman, 1978; Sausse
61 et al., 2001): in microfractures, where the leaching of solutes is less intense because transport
62 is associated to chemical gradients, the most common secondary products are smectites and
63 vermiculites; in fractures the leaching is intensified because solutes are carried away by the
64 flowing water and, as a consequence allophone and/or halloysite are formed; if velocity
65 and(or) the volume of flow increase, the leaching of (earth)alkaline elements and silica may
66 become extreme, resulting in formation of gibbsite.
67 Dissolution of parent minerals and precipitation of secondary products within microsystems
68 is accompanied by the alteration of rock porosity and permeability. In the process of chemical
69 weathering, water increasingly invades the microsystems developing secondary porosity that,
70 regardless of the quantities of the newly formed phases, generally increases because the
71 alteration products never completely replace the dissolved volume (Putnis, 2002; Meunier et

al., 2007). The increase in porosity changes the geometrical parameters of the pathways. Microfractures tend to widen and connect to other microsystems, increasing permeability (Sardini et al., 2001; Sausse et al., 2001). In later stages of weathering, associated to the development of saprolites, the microstructure of the rocks tends to disappear by collapsing or sliding under gravity, causing a substantial decrease in permeability, but not in porosity (Wright and Burgess, 1992).

Weathering studies based on the microsystem concept have been performed at the microscopic scale (Meunier and Velde, 1979; Hochella and Banfield, 1995; Sausse et al, 2001; Meunier et al., 2007), using thin sections of rock samples as investigating materials.

The main goal of this paper is to extrapolate the analysis of microsystems to the macroscopic scale, applying it to fault zones underlying a soil plus saprolite cover. The selection of fault zones to study the macroscopic behaviour of microsystems is adequate, because fault zones are complex fractured environments composed of large gravity-flow fractures in hydraulic connection with a network of small gravity-flow fractures and capillary-flow microfractures (rock matrix). At the scale of a fault zone, the evolution of pathway parameters can be described by hydraulic diffusivity, which is the ratio of hydraulic transmissivity (a proportion of permeability) to the storage capacity (a function of porosity). The aim is to verify if changes in the hydraulic diffusivity have an effect on the type of secondary minerals formed by weathering of plagioclase.

A complementary objective of this study is to calculate plagioclase weathering rates, taking into account particularities of the fractured rocks relative to groundwater travel time and area exposed to groundwater. The aim is to verify if the relation between weathering rates and groundwater travel time can also be described in terms of progressive hydraulic diffusivity changes.

2. Study Area

The region of Vila Pouca de Aguiar is located in the North of Portugal and occupies an area of approximately 437 km^2 (Figure 1). It is characterized morphologically by large-scale tectonic valleys, associated to the so-called Vila Real fault, surrounded by the Alvão (to the West) and Padrela (to the East) mountains. Altitudes range from a minimum of 200 m in the Northern valleys and a maximum of 1200 m up in the mountains.

Climate in the area is temperate with wet–cold and dry–warm alternating seasons. The annual precipitations range from 900 $mm \cdot yr^{-1}$ in the Northeast to 1900 $mm \cdot yr^{-1}$ in the Southwest of the region (Figure 2), being influenced by the topography.

The geology of the area is characterized by Hercynian (syn- to post-tectonic) granites that intruded Palaeozoic (Cambrian to Devonian) metassediments and were covered by Quaternary alluvial and terrace deposits along the Vila Real fault (Figure 2). In the Southeast part of the area, occupied by an extensive outcrop of metassediments, a geological structure was defined, in which tectonic laminae are folded and separated by major thrusts (Pacheco et al., 1997).

The Vila Pouca de Aguiar granites are composed of (in weight %) quartz (31.5), plagioclase (35.3), K-feldspar (26.7), biotite (4.4) and muscovite (1.4), with minor amounts of apatite and ilmenite. The plagioclase composition ranges from albite-An_8 to andesine-An_{37} (Pacheco et al., 1999). The metassediments, which include greywackes, phyllites, quartzites and graphitic slates, contain quartz, muscovite and smaller amounts of biotite, K-feldspar and albite-oligoclase (Pacheco, 1995).

121 *3. Hydrogeologic Setting*

122

123 *3.1. Conceptual Flow and Weathering Models*

124 The fate of infiltrated rainwater in a fractured massif comprises lateral flow through the
125 bedrock cover (soil and saprolite) and recharge. Recharge includes refilling of the rock
126 matrix, composed of a network of small gravity flow fractures and capillary flow
127 microfractures, and of fault zones composed of large gravity-flow fractures and crushed rock.
128 Figure 3 illustrates the lateral flow of shallow groundwater through a saprolite horizon with a
129 thickness z_0 (m), succeeded by its infiltration into a couple of sub-vertical fault zones. It also
130 shows paths of groundwater through the rock matrix until they reach the same fault zones.
131 Similar models of groundwater flow through fractured rocks towards fault zones have been
132 adopted by Herbert et al. (1992) and Verweij (1995).
133 The saprolite horizon is assumed an open system given the high effective porosity and
134 sometimes (granite saprolites) also high hydraulic conductivity of the disaggregated
135 materials. Depending on precipitation (P, mm), which determines the volume of flow,
136 secondary products expected to result from weathering of plagioclase are halloysite (lower
137 precipitations) or gibbsite (higher precipitations). In Portugal, gibbsite is the most common
138 secondary product for annual precipitations higher than about 1000 $mm \cdot y^{-1}$, whereas for
139 precipitations lower than this limit the dominant product is halloysite (Martins et al., 1995).
140 The fault zones are also assumed open systems because large gravity-flow fractures dominate
141 in these environments. However, no extreme flushing conditions are expected to occur given
142 the compaction of these zones caused by the burden of overlying rocks. For that reason,
143 plagioclase weathering is expected to produce halloysite. Finally, the rock matrix is assumed
144 a semi-open system given the dominance of small gravity-flow fractures and capillary-flow

145 microfractures in this environment. In this case, halloysite and smectite are both assumed
146 products of plagioclase weathering (Meunier et al., 2007).
147
148 *3.2. Boreholes*
149 In the past three decades, about 50 to 60 wells were drilled in the region of Vila Pouca de
150 Aguiar to be used as sources of drinking water for public supply. The location of 31 of the
151 most productive boreholes is plotted in Figure 1 (labelled circles) and the information on
152 name (Id), intersected rock type (granite or metassediment), depth (z, m), slope of the
153 topographic surface (d in %, sampled from the Digital Elevation Model of Figure 1) and local
154 precipitation (P in $mm \cdot y^{-1}$, sampled from Figure 2), is depicted in Table 1. The associated
155 yields are illustrated in Figure 2 and can be justified by a combination of factors
156 encompassing the high annual precipitation, the abundance of quartzites within the
157 metassediments, and especially the proximity of the borehole to the Vila Real fault, to folds
158 and thrusts, or to the contact between granites and metamorphic rocks, places where the
159 fracture sets are usually more dense and interconnected. A number of studies reported the
160 proximity of boreholes to densely fractured regions as an important cause for observed high
161 yields (Siddiqui and Parizek, 1971; Mabee, 1999; Neves and Morales, 2007; among others).
162 During the drillings, several gravity-flow fractures were intersected by the boreholes
163 releasing variable amounts of water. The depth of intersection of fracture i (z_i, m) and its
164 corresponding yield (Q_i, $m^3 \cdot h^{-1}$) are listed in Table 1 for the above mentioned 31 boreholes.
165 Depths of intersection and yields were reported by the well drillers. For the first fracture, the
166 depth was set when water started flowing upward through the borehole emerging naturally at
167 the surface. For the other fractures of the same borehole, depths were set when an increase in
168 the natural outflow was noted. Yields were determined as the rate of water that can be
169 airlifted on a continuous short-term (generally tens of minutes) basis. These approaches for

estimating fractured aquifer depths and yields are common and have been used in many other studies (e.g., Moore et al., 2002). The average depth of the gravity flow fractures (z_{med}, m) was estimated by weighting the depth of each fracture according to its yield:

$$z_{med} = \frac{\Sigma_{j=1}^{n} z_j Q_j}{\Sigma_{j=1}^{n} Q_j} \quad (1)$$

where n is the number of fractures intersected by the borehole.

3.3. Pumping Tests and Hydraulic Parameters

Pumping tests were conducted on 14 of the 31 boreholes, lasting in all cases but one from 1140 to 2760 minutes. The exception was the test conducted on borehole Nr 22 (Cevivas) which ran for just 330 minutes. The duration of the tests and their pumping rates and hydrostatic levels are listed in Table 2.

In all cases, the scatter points drawdown (s, m) *versus* time (t, min) in a semilogarithmic plot could be fitted with a straight line, after the first 100 minutes of pumping. In three cases (tests to boreholes Nr 4, 19 and 20), the points could be linearly fitted with different two slopes, the first after 10 minutes of pumping and the second after 100 minutes of pumping. Figure 4 illustrates the test to borehole Nr 4. The fitting of (s,t) points to one straight line in a semilogarithmic plot is conform with type curves derived for porous media aquifers, and for that reason aquifer transmissivities (T, $m^2 \cdot s^{-1}$) based on the straight lines fitted to the after-10 and/or after-100 minutes period(s) were calculated using a classical porous media model (the Cooper-Jacob, 1946, formula):

$$T = \frac{2.3Q}{4\pi\Delta s} \quad (2)$$

where Q ($m^3 \cdot s^{-1}$) is the pumping rate and Δs (m) the change in s corresponding to a log cycle of time. The two fittings reported for boreholes Nr 4, 19 and 20 can be attributed to heterogeneity of the tested rocks: boreholes drain several gravity-flow fractures, with

194 different hydraulic heads, that apparently reacted to pumping at two different moments
195 during the test. The influence of rock heterogeneity on pumping test results and interpretation
196 has been quoted by Dagan (1986), Newman (1990), Belcher et al. (2001), Kollet and Zlotnik
197 (2005), among other workers.
198 The hydraulic diffusivity (D, $m^2 \cdot s^{-1}$) is the quotient of transmissivity (T, $m^2 \cdot s^{-1}$) and storage
199 coefficient (S, dimensionless):
200 $$D = T/S \quad (3)$$
201 Fractured rocks and regoliths derived therefrom span a wide range of D values, as depicted in
202 Table 3. The hydraulic conductivity (K, $m \cdot s^{-1}$) is the quotient of transmissivity and the
203 drainable thickness (b, m):
204 $$K = T/b \quad (4)$$
205 The drained thicknesses of the tested boreholes are listed in Table 2 and were estimated by
206 multiplying the number of intersected fractures (Table 1) by the length of the screened tubes
207 casing the borehole around those fractures (in general 6 m, but 3 or 1 m for boreholes
208 Cevivas and Santa Marta, respectively). Effective porosity (n_e, dimensionless) is the volume
209 of connected voids in a sample divided by the total volume of the sample, and can be derived
210 from the storage coefficient (Domenico and Schwartz, 1998):
211 $$n_e = \frac{S}{\rho_w b \sigma_w} \quad (5)$$
212 where ρ_w is the specific weight of water (999.1 $kg \cdot m^{-3}$ at T = 15ºC) and σ_w the
213 compressibility coefficient of water (4.7×10^{-9} $m^2 \cdot kg^{-1}$).
214 *4. Sampling and Analysis*Samples of borehole water were collected within the limits of the
215 Vila Pouca de Aguiar municipality from January 2006 to April 2006. The sampling sites are
216 shown in Figure 1. At the sampling site, electrical conductivity (EC), temperature (T, ºC) and
217 pH were measured and a water sample was filtered through a 0.4 μm membrane filter. The

filtered water was split into 2 portions; one was stored for analysis in the home laboratory, acidified to pH 2 using pure nitric acid, and the other for analysis of alkalinity in the field laboratory, within 24 hours using the Gran plot method. In the home laboratory, ICP-OES was used for analysis of Si. The analytical results are shown in Table 4.

5. Weathering Reactions and Rates

Not all minerals present in the granites or in the metassediments are important as weathering reactants. In general, the abundance of plagioclase in granites is significant and therefore the relative contribution of plagioclase weathering to groundwater composition is expected to be expressive. However, because plagioclase has a low resistance to weathering, when compared to other minerals composing these rocks (e.g. quartz, biotite, muscovite; Bland and Rolls, 1998; Appelo and Postma, 2005), this relative contribution may not be just expressive but dominant. For example, in granite areas of central Portugal, Pacheco and Van der Weijden (1996) and Van der Weijden and Pacheco (2006) reported contributions greater than 90%. In the Vila Pouca de Aguiar granites, this dominance was also recognised by Pacheco et al. (1999), which reported contributions between 95 and 98%, and of 99% when weathering was associated to fault zones. In the metassediments, plagioclase may be present solely in small amounts. However, weathering of plagioclase may also contribute dominantly to ground water composition, because the surrounding minerals (e.g. quartz, chlorite) are usually much less reactive. For example, in an area with metassediments where groundwater chemistry was explained by weathering of plagioclase (albite) and chlorite (Pacheco and Alencoão, 2006), the abundance of chlorite is about twice the abundance of albite, but on average the relative contribution of albite weathering to groundwater composition is greater than 90%. For the

242 reasons described above, it is assumed in this case that plagioclase weathering explains the
243 natural composition of ground water, namely the concentrations of silica and bicarbonate.
244
245 *5.1. Mass Balances*
246 Reactions of plagioclase producing gibbsite, halloysite, or smectite are listed in Table 5. The
247 contribution of each reaction to groundwater composition can be accomplished by solving a
248 set of mole balance equations based on the reaction stoichiometries, namely on the
249 bicarbonate to dissolved silica ratio (*r*) which is a key parameter in distinguishing between
250 different reactions (Garrels, 1967; Pacheco and Van der Weijden, 1996). For the reactions
251 listed in Table 5, the ratios are:

252 $$r_{\mathrm{Gibb}} = \frac{1+x}{3-x} \quad (6a)$$

253 $$r_{\mathrm{Hal}} = \frac{1}{2}\frac{1+x}{1-x} \quad (6b)$$

254 $$r_{\mathrm{Sm}} = \frac{0.6(1+x)}{0.95-5.65x} \quad (6c)$$

255 where x is the anorthite content of plagioclase ($0 \le x \le 1$), and the mole balance equations
256 are:

257 $$\left[HCO_3^-\right] = r_{\mathrm{Gibb}}[H_4SiO_4^0]_{\mathrm{Gibb}} + r_{\mathrm{Hal}}[H_4SiO_4^0]_{\mathrm{Hal}} + r_{\mathrm{Sm}}[H_4SiO_4^0]_{\mathrm{Sm}} \quad (7a)$$

258 $$[H_4SiO_4^0] = [H_4SiO_4^0]_{\mathrm{Gibb}} + [H_4SiO_4^0]_{\mathrm{Hal}} + [H_4SiO_4^0]_{\mathrm{Sm}} \quad (7b)$$

259 where square brackets represent dissolved concentrations. The unknowns of the system are x
260 and the partial concentrations of dissolved silica. An average value for x can be obtained
261 from chemical analysis of granite and metassediment plagioclases (in the Vila Pouca de
262 Aguiar region, plagioclase is faithfully represented by an oligoclase, meaning that $x \approx 0.2$).
263 However, to become a determined system, set 7a,b must be completed with an additional
264 equation.

According to the conceptual flow and weathering models illustrated in Figure 3, the concentration derived from reaction R_{Gibb} ($[H_4SiO_4^0]_{Gibb}$) is released when shallow groundwater moves along the saprolite path, whereas the concentrations derived from R_{Hal} ($[H_4SiO_4^0]_{Hal}$) and R_{Sm} ($[H_4SiO_4^0]_{Sm}$) are released or consumed along the fault zone plus rock matrix paths. In the first case, the movement of water is sideways and water-mineral interactions occur within a relatively narrow depth range (from ground surface to z_0). Solute concentrations will be higher or lower depending on whether the length of the saprolite flow path is longer (*lsp* in Figure 3) or shorter (*ssp*), but they will be independent of circulation depth (z). In the second case, water moves laterally as well as vertically, being sampled in the boreholes at a depth $z = z_{med}$. The value of z_{med} varies from place to place (e.g., from 18 to 96 meters in the study area, Table 1). If dissolution of plagioclase and transport of silica along the fault zone plus rock matrix paths are assumed continuous, then a range in circulation depths are expected to follow a concomitant range in the dissolved silica concentrations, the overall result being a regression between $[H_4SiO_4^0]_{Hal} + [H_4SiO_4^0]_{Sm}$ and z_{med}. This relationship is not universal but can be defined for each particular case. With this relation added to Equations 7a,b, the set becomes determined, and a unique solution can be found for its unknowns.

5.2. Moles of Dissolved Plagioclase

The moles of plagioclase ([Pl]) dissolved along the saprolite, fault zone and rock matrix flow paths are obtained by multiplying the concentrations of silica derived from reactions R_{Gibb}, R_{Hal} and R_{Sm} by the concomitant plagioclase to silica ratios (β), as deduced from Table 5:

$$[Pl] = \beta_{Gibb}[H_4SiO_4^0]_{Gibb} + \beta_{Hal}[H_4SiO_4^0]_{Hal} + \beta_{Sm}[H_4SiO_4^0]_{Sm} \quad (8)$$

where

$$\beta_{Gibb} = \frac{1}{3-x} \quad (9a)$$

290 $$\beta_{Hal} = \frac{1}{2(1-x)} \quad (9b)$$

291 $$\beta_{Sm} = \frac{1.65}{0.95-5.65x} \quad (9c)$$

292 The first term of the right-hand side of Equation 8 represents the number of moles of
293 plagioclase dissolved along the saprolite path ($[Pl]_0$) whereas the sum of the second and third
294 terms represent the moles dissolved along the fault zone plus rock matrix paths.

295

296 *5.3. Plagioclase Weathering Rates*

297 Weathering rates of plagioclase can be estimated using:

298 $$W_{Pl} = \frac{[Pl]-[Pl]_0}{t} \times \frac{V_r}{A_{Pl}} \quad (10)$$

299 where W_{Pl} ($mol \cdot m^{-2} \cdot s^{-1}$) is the rate and $[Pl]-[Pl]_0$ ($mol \cdot m^{-3}$) its concomitant dissolved
300 concentration, t (s) is the average groundwater travel time of water packets flowing through
301 the fault zone and through the rock matrix, V_r ($m^3 \cdot s^{-1}$) is the volume of water entering the
302 fault zone in a unit time, and A_{Pl} ($m^2 \cdot s^{-1}$) is the surface area of plagioclase in contact with that
303 volume of aquifer water. An equation for A_{Pl} was developed by Pacheco and Alencoão
304 (2006), describing the area of fracture surfaces in contact with aquifer water in unit time:

305 $$A_{Pl} = 2\alpha_{Pl} V_r \times \sqrt{\frac{\rho_w g n_e}{12 \mu_w K}} \quad (11)$$

306 where α_{Pl} is the proportion of plagioclase in the rock, μ_w (1.14×10^{-3} $kg \cdot s^{-1} \cdot m^{-1}$ at T = 15ºC)
307 is the dynamic viscosity of water, and g is the acceleration of gravity (9.81 $m \cdot s^{-2}$). Replacing
308 this equation in Equation 10 and rearranging gives:

309 $$W_{Pl} = \frac{[Pl]-[Pl]_0}{2t\alpha_{Pl}} \sqrt{\frac{12\mu_w K}{\rho_w g n_e}} \quad (12a)$$

310 Further substitution of Equation 5 in Equation 12a gives

311 $$W_{Pl} = \frac{[Pl]-[Pl]_0}{2t\alpha_{Pl}} C_w \sqrt{D} \quad (12b)$$

where

$$C_w = \sqrt{\frac{12\mu_w\sigma_w}{g}} = 2.56\times10^{-6}\ \text{s}^{1/2}\ (\text{at } T = 15^{\circ}\text{C}) \quad (12c)$$

Equation 12b describes the weathering rate as an explicit function of hydraulic diffusivity.

6. Groundwater Travel Times

The average groundwater travel time is the length of the flow path divided by the mean velocity of water along that path. According to the conceptual flow model (Figure 3), water will move towards the fault zones following two distinct paths: the fault zone path or the rock matrix path. The length of the fault zone path can be equated to $z_{med}-z_0$, assuming that fault zones are almost vertical, where z_{med} is the average depth to the conductive fractures (Equation 1) and z_0 is the thickness of the saprolite layer. The length of the rock matrix path is difficult to assess, because it depends on the average distance between the recharge areas and the fault zones as well as on the tortuosity of the path, which are unknowns. In this study, the length of the flow path was approached to $z_{med}-z_0$. This provides minimum values for flow path lengths and consequently to groundwater travel times, maximizing weathering rates (Equation 12). Difficulties in determining the rock matrix flow path length were also encountered and not resolved by Meunier et al. (2007). The mean velocity of water along the flow path (v, $\text{m}\cdot\text{s}^{-1}$) is (Domenico and Schwartz, 1998):

$$v = \frac{Ki}{n_e} \quad (13)$$

where i is the hydraulic gradient (dimensionless). Although hydraulic gradients are influenced by recharge and discharge rates as well as by groundwater withdrawal, they follow primarily the local relief (Appelo and Postma, 2005), being determined by the slope of the topographic surface (d, dimensionless). Hence, the travel time of groundwater moving from

the bottom of the saprolite layer till the average depth of conductive fractures can be written as:

$$t = \frac{(z_{med} - z_0)n_e}{Kd} \quad (14)$$

It should be mentioned that K and n_e were estimated from results of long-term pumping tests, and therefore correspond to an average of the hydraulic conductivities and effective porosities of the fault zone plus rock matrix.

7. Results and Discussion

7.1. Hydraulic Tests

The hydraulic test of borehole Bornes 1 (Figure 4) ran at a pumping rate $Q = 13.5\times10^{-3}$ $m^3 \cdot h^{-1}$ (Table 2). For the log cycle 10 to 100 minutes, the scatter points fit to a straight line with drawdowns $s_{10} = 2.5$ and $s_{100} = 7.8$ m, respectively. The change in the drawdown is $\Delta s_1 = 5.3$ m which results in $T_1 = 1.31\times10^{-4}$ $m^2 \cdot s^{-1}$ (Equation 2). For the next log cycle of time (100 to 1000 minutes) the scatter points fit to a less inclined straight line resulting in a smaller $\Delta s_2 = 2.3$ m and a larger transmissivity $T_2 = 3.05\times10^{-4}$ $m^2 \cdot s^{-1}$. Even though the time spans linked to T_1 and T_2 are usually different (Figure 4), the average fault zone transmissivities were calculated using the arithmetic mean $(T_1+T_2)/2$. For the fault zone intersected by borehole Bornes 1, $T_{med} = 2.18\times10^{-4}$ $m^2 \cdot s^{-1}$. When considering the results of all pumping tests, $T_{med} = (1.5\pm1.2)\times10^{-4}$ $m^2 \cdot s^{-1}$. There were no observation wells around the tested boreholes so a reasonable value had to be found for the storage coefficient. The choice was the average storage coefficient of a 33.2 m thick fault zone estimated by Pacheco (2002): $S = (7.75\pm1.71)\times10^{-5}$. Standing on this coefficient, the hydraulic diffusivities were calculated by Equation 3 and compiled in Table 4. On average, $D = 1.7\pm1.4$ $m^2 \cdot s^{-1}$. These values lie in a range of values observed for fractured weathered crystalline rocks (0.1–10 $m^2 \cdot s^{-1}$; Table 3)

and are in agreement with results obtained in other studies (Talwani, 1981; Talwani and Acree, 1984; Rastogi et al., 1986; Shapiro et al, 1997; Talwani and Cobb, 1999).

For borehole Bornes 1, b = 18 m and so $K_{med} = 12.1\times10^{-6}\ m\cdot s^{-1}$ (Equation 4). For the entire set of tested wells $K_{med} = (8.8\pm5.7)\times10^{-6}\ m\cdot s^{-1}$ (Table 2). Hydraulic conductivities decrease steadily with z_{med} as shown in Figure 5. The scatter points in this figure can be fitted to an exponential function:

$$K(\times10^{-6}\,m\cdot s^{-1}) = 53.37e^{-0.051z_{med}},\ R^2 = 0.7 \quad (15)$$

This equation was used to estimate hydraulic conductivities for the non-tested boreholes (Table 4). The effective porosity was based on the adopted storage coefficient ($S = 7.75\times10^{-5}$), and was estimated using Equation 5. The result was: $n_e = 0.50$.

7.2. Weathering Reactions

The physicochemical parameters of the sampled waters are given in Table 4. During the saprolite, fault zone and rock matrix paths, reaction of water with rock forming minerals releases solutes and precipitates clay minerals, hydroxides, etc. One of the reaction-derived solutes is silica ($H_4SiO_4^0$) and for the studied borehole waters the concentrations of $H_4SiO_4^0$ ($mol\cdot L^{-1}$) increase with depth (z_{med}, Figure 6). The sympathy between $[H_4SiO_4^0]$ and z_{med} is clear, in spite of the scatter bounded by two dashed lines. This scatter can be ascribed to the contribution of saprolite weathering to $[H_4SiO_4^0]$, i.e. to weathering occurring before the entrance of shallow ground water into the rock matrix and fault zones intersected by the drilled wells, because this contribution is not supposed to depend on z_{med}. According to the conceptual weathering model described before, the saprolite contribution to weathering is referred to as $[H_4SiO_4^0]_{Gibb}$. Since water moves laterally along the saprolite path (Figure 3), interacting with minerals within a narrow range of circulation depths (0–z_0 meters), there is

no reason why $[H_4SiO_4^0]_{Gibb}$ should depend on z_{med}. Instead, $[H_4SiO_4^0]_{Gibb}$ should vary in agreement with changes in the saprolite path length, as interpreted from a detailed analysis of Figure 6. In this figure, we shall presume that $[H_4SiO_4^0]_{Gibb}$ is represented by a point in the dotted line. This line marks the intersection between the lower dashed line and the X-axis (z_0) and stands for the average thickness of the saprolite layer (z_0 = 16 m). If the path followed by groundwater during the stage of saprolite weathering is the largest (*lsp* in Figure 3) then $[H_4SiO_4^0]_{Gibb}$ is also the largest and represented by the intersection between the upper dashed line and the dotted line. If this path is the shortest (*ssp*) then $[H_4SiO_4^0]_{Gibb}$ will approach zero and be represented by the intersection between the lower dashed line and the dotted line. In general (values in Table 4),

$$[H_4SiO_4^0]_{Gibb} = [H_4SiO_4^0] - 0.0043(z_{med}-z_0) \quad (16)$$

where 0.0043 is the slope of the dashed lines.

For the present case study, Equation 16 is required to convert Equations 7a,b into a set with a unique solution for $[H_4SiO_4^0]_{Hal}$ and $[H_4SiO_4^0]_{Sm}$.

The concentrations of silica derived from reactions R_{Gibb}, R_{Hal} and R_{Sm} (Table 5) are listed in Table 4. In all cases $[H_4SiO_4^0]_{Gibb}$ and $[H_4SiO_4^0]_{Hal}$ are positive, meaning that the corresponding reactions invariably release silica to solution. With four exceptions (samples from drilled wells Nr 11, 12, 17 and 26), $[H_4SiO_4^0]_{Sm}$ is negative, meaning that R_{Sm} generally consumes silica from solution. These results are in keeping with the equations for the *r* ratios (Equations 6a–c), because for any value of x r_{Gibb} and r_{Hal} are positive while r_{Sm} is positive only for x < 0.056 (albite). The exceptions represent cases where adoption of x = 0.2 is inadequate. For the cases where R_{Sm} consumes silica, the reaction proceeds only if there is some silica available in the solution, for example transported along the flow path from places where

weathering of plagioclase has released this solute, i.e. from places where R_{Gibb} or R_{Hal} were the prevailing reactions.

7.3. Weathering Reactions and Hydraulic Diffusivity

A plot of silica concentrations derived from reactions R_{Hal} and R_{Sm} (Table 5) *versus* hydraulic diffusivity (D) is illustrated in Figure 7. For silica released by R_{Hal}, concentrations decrease as D increases, according to a power function. When silica is consumed by R_{Sm}, this consumption increases for increasing values of D, according to a linear function.

Fault zones are low diffusive environments because water tends to follow large gravity fractures (the easiest routes). Contrarily, the rock matrix is potentially a high diffusive environment because water has to move in a network of connected small gravity flow fractures and capillary flow microfractures; the higher the connectivity the higher the hydraulic diffusivity (Knudby and Carrera, 2006). According to this setting, fault zones must be plotted to the left-hand side of Figure 7 and the rock matrix to the right-hand side of that diagram. The boundary between the two environments must be drawn in keeping with the conceptual weathering model described before. According to this model, reactions involving plagioclase and occurring along fault zones (completely open systems) should be related to precipitation of halloysite, and reactions occurring along the rock matrix (semi-open system) to precipitation of smectite plus halloysite. In Figure 7, this scenario becomes more evident for $D \approx 0.7$ $m^{-2} \cdot s^{-1}$: when $D < 0.7$ $m^{-2} \cdot s^{-1}$, concentrations derived from R_{Hal} are high (average: 280 $mmol \cdot L^{-1}$) and concentrations related to R_{Sm} approach zero (average: −16 $mmol \cdot L^{-1}$); for $D > 0.7$ $m^{-2} \cdot s^{-1}$, both reactions play a role in weathering of plagioclase (the average concentrations are 158 $mmol \cdot L^{-1}$ for R_{hal} and −67 $mmol \cdot L^{-1}$ for R_{sm}), with a growing relative importance of R_{Sm}. Although the limit of $D = 0.7$ $m^{-2} \cdot s^{-1}$ may be considered arbitrary, it

certainly can be used as provisional threshold for the separation between fault zone (open system) and rock matrix (semi-open system) weathering.

An association can also be recognized between precipitation of halloysite and advective flow along gravity fractures of the fault zones and rock matrix. This is illustrated in Figure 8. No correlation exists between $[H_4SiO_4^0]_{Gibb}$ and z_{med}, but even was not expected as production of gibbsite is ascribed to the saprolite path, not to the fault zone or rock matrix paths. A correlation between the remainder of silica ($[H_4SiO_4^0]_{Hal}$ + $[H_4SiO_4^0]_{Sm}$) and z_{med} was already discussed (Figure 6) but Figure 8 shows that only $[H_4SiO_4^0]_{Hal}$ is correlated with depth. This is a remarkable result because confirms that production of halloysite is indeed associated with plagioclase weathering along the mean direction of flow, and that the same does not hold for production of smectite. In keeping with these results, it may be concluded that production of halloysite does occur along the walls of gravity-flow fractures, in fault zones or the rock matrix. In these two media, solute transport is advective and therefore concentrations must increase with increasing flow path lengths (z_{med}) justifying the observed correlation. Conversely, production of smectite occurs at micro fractures adjacent to the gravity flow fractures, where solute transport is diffusive, mediated by local gradients of chemical potential and by the length of diffusion trajectories between the capillary and gravity-flow fractures, and hence not necessarily dependent on the flow path lengths.

7.4. Groundwater Travel Times, Plagioclase Weathering Rates and Hydraulic Diffusivity

Groundwater travel times (t) calculated by Equation 14 are given in Table 4 and range from 0.01 to 13.7 years, being on average 2.2±3.5 yr. Plagioclase weathering rates (W_{Pl}) calculated by Equation 12b are compiled in Table 4, with an average logarithmic value of –12.9±1.1. These rates are plotted in Figure 9 (filled circles) along with field weathering rates reported in

456 other studies (White and Brantley, 2003, and references therein; open circles), with an
457 average logarithmic value of −15.1±1.0.
458 Literature rates are on average 2.2 orders of magnitude lower than the rates calculated in this
459 study. In a first glance at Figure 9, it could be suggested that factor time is the sole
460 explanation for this discrepancy, but a thorough analysis of the various results reveals that
461 other factors are also important. The open circles are mostly solid-state weathering rates
462 based on the differences between elemental, isotopic and mineral compositions measured in
463 present-day regoliths and in the assumed protolith. In these cases, variable *t* represents the
464 entire time span of a weathering episode, commonly on the order of thousands to million
465 years. The filled circles are solute-flux rates that stand for contemporary weathering during
466 groundwater percolation in the fractured rocks, in which case *t* (travel time) is just a portion
467 of that time window, frequently ranging from years to decades. For the open circles, it is
468 inherently assumed that the weathering environment is initially a fresh rock (the protolith),
469 i.e. a medium with a very high hydraulic diffusivity (Table 3). For the filled circles, it is
470 recognised that many groundwater parcels have circulated through the fractured rocks over
471 the full time span of weathering, which had as consequence a progressive decrease in the
472 hydraulic diffusivity, till present day values that do not exceed 5 $m^2 \cdot s^{-1}$ (Table 4).
473 The consequences for weathering rates of changing the hydraulic properties of the percolated
474 rocks are predicted by Equation 12b: the impact in the W_{Pl} values is proportional to the square
475 root of the change in the *D* values. To elucidate the full relationship between weathering rate,
476 hydraulic diffusivity and time, an equation describing the drop in *D* as a function of *t* has to
477 be defined. If, as working hypothesis, it is assumed that *D* decreases according to a power
478 function of *t*, then Equation 12b can be rewritten as:

479 $$W_{Pl} = \frac{[\mathrm{Pl}] - [\mathrm{Pl}]_0}{2(\eta t)\alpha_{\mathrm{Pl}}} C_w \sqrt{D_0 (\eta t)^{-f/\eta}} \qquad (17)$$

480 with t given in years and where f is the decreasing rate, η converts years into seconds (η
481 $=3.1536\times10^{7}$ s·yr^{-1}), and D_0 is a proxy for the initial hydraulic diffusivity. The plot of
482 Equation 17 in Figure 9 is represented by the dotted lines, each one representing a different
483 D_0. In this plot, it is assumed that $[Pl] - [Pl]_0 = 0.686$ mol·m^{-3} (the average value; Table 4),
484 that $\alpha_{Pl} = 0.353$ (the proportion of plagioclase in the granites) and that $f = 1$. According to the
485 distribution of the D_0 lines, most solid-state rates are indeed related to the weathering of a
486 protolith with $10^3 < D_0 < 10^6$ m^2/s whereas solute-flux rates are related to a weathered
487 fractured rock with $10^{-2} < D_0 < 10^2$ m^2/s. It is also clear that, in case the aquifers investigated
488 in this study were composed of average diffusivity protoliths ($D_0 = 10^5$ m^2·s^{-1}; Table 3),
489 instead of being composed of low diffusivity weathered fractured rocks ($D_0 \approx 10^0$ m^2·s^{-1};
490 Table 4), the calculated rates would be 2.5 orders of magnitude higher (A-double arrowed
491 line in Figure 9). This difference may be defined as the impact on weathering rates resulting
492 from continuous recirculation of groundwater through the studied fault zones, over the
493 geologic times. Factor time adds up to the previous impact, being minimal for waters that
494 circulated through the system only a few days or months and maximum for waters with
495 residence times of several years or decades. In the studied region, the difference between
496 minimum and maximum rates spans 4 orders of magnitude (B-double arrowed line). In
497 summary, the past changes in hydraulic diffusivity till present day values account for
498 approximately 40% reduction in weathering rates (2.5 orders of magnitude), relatively to their
499 presumed original values, whereas travel time accounts for the remaining 60% (4 orders).
500
501 *8. Conclusions*
502
503 The drawdown (s) in boreholes (observed during pumping tests), plotted against log cycles of
504 pumping time (t) could be fitted by two straight lines, one for a short (10 to 100 minutes), the

505 other for a longer (100 to 1000 minutes) period of pumping time. Using the latter results, the
506 average transmissivity (T) was estimated and, in combination with an average storage
507 coefficient (S) typical for regional fault zones, the hydraulic diffusivity ($D = T/S$) could be
508 calculated: on average $D = 1.7 \pm 1.4$ $m^2 \cdot s^{-1}$. Lower values of D are typical for fault zones with
509 large fractures, while higher values are indicative of connected networks of small to very
510 small fractures typical for the rock matrix. Applying the so-coined SiB mass balance
511 equations (Pacheco and Van der Weijden, 1996) to the water composition, the contribution of
512 dissolved plagioclase to the water chemistry as well as the amounts of secondary precipitates
513 (gibbsite, halloysite, smectite) withdrawn from these waters can be calculated. Next, the net
514 release of dissolved silica from plagioclase dissolution in combination with precipitation of
515 gibbsite and halloysite and its consumption by smectite formation can be computed. The net
516 release of dissolved silica derived from plagioclase dissolution in combination with halloysite
517 precipitation correlates with the average depth (z_{med}) of the productive sectors of the drilled
518 wells, strongly suggesting halloysite precipitation along fractures in the bedrock.
519 Combinations of dissolved silica concentrations derived from plagioclase dissolution with
520 precipitation of gibbsite or smectite lack a correlation with z_{med}. The relation between the net
521 dissolved silica concentrations and D suggests that for $D < 0.7$ $m^2 \cdot s^{-1}$ the weathering of
522 plagioclase is largely followed by precipitation of halloysite and takes place in the completely
523 open system of the fault zone, whereas at higher values reactions occur also in the rock
524 matrix with precipitation of both halloysite and smectite. Groundwater travel times are on
525 average 2.2±3.5 year. Weathering rates (W_{Pl}*'s*) are calculated from the moles of plagioclase
526 dissolved along the flow path per unit of area of plagioclase exposed to the fluid and travel
527 time t. The average $(W_{Pl}) = 10^{-(12.9 \pm 1.1)}$ $mol \cdot m^2 \cdot s^{-1}$ is 2.2 orders of magnitude higher than
528 solid-state weathering rates reported in various studies. The explanations for the apparent
529 discrepancy are partly the past changes in hydraulic diffusivity of the weathering

530 environments, from approximately 10^5 m^2/s in the protoliths to 0.1–1 m^2/s in present-day
531 weathered fractured rocks, and partly the duration of weathering.
532

533 **References**

534

535 Abrisqueta, J. M., Plana, V., Ruiz-Canales, A., Ruiz-Sánchez, M. C, 2006. Unsaturated hydraulic
536 conductivity of disturbed and undisturbed loam soil. Span. J. Agric. Res. 4(1), 91–96.

537

538 Appelo, C.A.J., Postma, D., 2005. Geochemistry, Groundwater and Pollution. A.A. Balkema,
539 Rotterdam, 649 pp.

540

541 Baynes J., Dearman, W.R., 1978. The microfabric of a chemically weathered granite. Bull. Eng. Geol.
542 Environ.18, 91−100. doi: 10.1007/BF02635354

543

544 Belcher, W.R., Elliott, P.E., Geldon, A.L., 2001. Hydraulic-property estimates for use with a transient
545 ground-water flow model for the Death Valley regional ground-water flow system, Nevada and
546 California: U.S. Geological Survey Water-Resources Investigations Report 01−4210. url:
547 http://water.usgs.gov/pubs/wri/wri014210/.

548

549 Bland, W., Rolls, D., 1998. Weathering: and Introduction to the Scientific Principles. Arnold, London,
550 271p.

551

552 Cooper, H.H., Jacob, C.E., 1946. A generalized graphical method for evaluating the formation
553 constants and summarizing well field history. Transactions American Geophysical Union 27,
554 526−534.

555

556 Dagan, G., 1986. Statistical theory of groundwater flow and transport: Pore to laboratory, laboratory
557 to formation, and formation to regional scale. Water Resour. Res. 22(9), 120S−135S.
558 doi:10.1029/WR022i09Sp0120S

559

560 Domenico, P.A., Schwartz, F.W., 1998. Physical and Chemical Hydrogeology (2nd ed.). John Wiley &
561 Sons Inc., New York, 506pp. doi: wiley.com/ 10.1002/ 1099-1034(200004/ 06)35
562
563 Garrels, R.M., 1967. Genesis of some ground waters from igneous rocks. In: Abelson, P.H. (Ed.),
564 Researches in Geochemistry, Wiley, New York, v. 2, pp. 405–420.
565
566 Herbert, R., Barker, J.A., Kitching, R., 1992. New approaches to pumping test interpretation for dug
567 wells constructed on hard rocks. In: Burgess, E.P. (Ed.), Hydrogeology of crystalline basement
568 aquifers in Africa. Geological Society Special Publication, no. 66, pp. 221–242. doi: 10.1144/
569 GSL.SP.1992.066.01.11.
570
571 Hochella, M.F., Banfield, J.F., 1995. Chemical weathering of silicates in nature: a microscopic
572 perspective with theoretical considerations. In: White, A.F. & Brantley, S.L. (Eds.), Chemical
573 Weathering Rates of Silicate Minerals. Reviews in Mineralogy 31, Mineralogical Society of America,
574 pp. 353–406.
575
576 Knudby, C., Carrera, J., 2006. On the use of apparent hydraulic diffusivity as an indicator of
577 connectivity. J. Hydrol. 329, 377–389. doi:10.1016/j.jhydrol.2006.02.026.
578
579 Kollet, S.J., Zlotnik, V.A., 2005. Influence of aquifer heterogeneity and return flow on pumping test
580 data interpretation. J. Hydrol. 300(1−4), 267–285. doi:10.1016/j.jhydrol.2004.06.011.
581
582 Korzhinskii, D.S., 1959. Physicochemical Basis of the Analysis of the Paragenesis of Minerals
583 (translation). Consultant Bureau, New York, 143 p.
584
585 Mabee, S.B., 1999. Factors influencing well productivity in glaciated metamorphic rocks.
586 Groundwater 37(1), 88–97. doi: 10.1111/j.1745-6584.1999.tb00961.x.

587 Martins, A.A.A., Madeira, M.V., Refega, A.A.G., 1995. Influence of rainfall on properties of soils
588 developed on granite in Portugal. Arid Soil Res. Rehabil. 9, 353–366. doi:
589 10.1080/15324989509385904.
590
591 Meunier, A., Velde, B., 1979. Weathering mineral facies in altered granites: the importance of local
592 small-scale equilibria. Mineral. Mag, 43, 261–268.
593
594 Meunier, A., Sardini, P., Robinet, J.C., Prêt, D., 2007. The petrography of weathering processes: facts
595 and outlooks. Clay Miner. 42, 415–435. doi: 10.1180/claymin.2007.042.4.01
596
597 Moore, R.B., Schwarz, G.E., Clark Jr., S. F., Walsh, G.J., Degnan, J. R., 2002. Factors Related to
598 Well Yield in the Fractured-Bedrock Aquifer of New Hampshire. U.S. Geol. Survey Prof. Paper 1660,
599 22p.
600
601 Neuman, S.P., 1975. Analysis of pumping test data from anisotropic unconfined aquifers considering
602 delayed gravity response. Water Resour. Res. 11(2), 329–342.
603
604 Neves, M.A., Morales, N., 2007. Structural control over well productivity in the Jundiaí River
605 Catchment, Southeastern Brazil. Annals of the Brazilian Academy of Sciences 79(2), 307–320.
606
607 Pacheco, F.A.L., 1995. Interacção Água-Rocha em Unidades do Grupo Peritransmontano (Serra da
608 Padrela-Vila Pouca de Aguiar). MSc Thesis, Coimbra University, Coimbra, 123p.
609
610 Pacheco, F.A.L., 2002. Response to pumping of wells in slopping fault-zone aquifers. J. Hydrol.
611 259(1–4), 116–135. doi: 10.1016/S0022-1694(01)00584-4
612

613 Pacheco, F.A.L., Alencoão, A.M.P., 2006. Role of fractures in weathering of solid rocks: narrowing
614 the gap between experimental and natural weathering rates. J. Hydrol. 316, 248–265.
615 doi:10.1016/j.jhydrol.2005.05.003.
616
617 Pacheco, F.A.L., and Van der Weijden, C.H., 1996. Contributions of water-rock interactions to the
618 composition of groundwater in areas with a sizable anthropogenic input. A case study of the waters of
619 the Fundão area, central Portugal. Water Resour. Res. 32(12), 3553–3570. doi:10.1029/96WR01683.
620
621 Pacheco, F.A.L., Sousa, L.M.O., Sousa Oliveira, A., 1997. The Supply of a Small Town with
622 Groundwater from Thrusted Quartzites. In: Marinos, P.G. et al. (eds.), Engineering Geology and the
623 Environment, Balkema, Rotterdam, v. 2, pP. 1407−1412.
624
625 Pacheco, F.A.L., Sousa Oliveira, A., Van der Weijden, A.J., Van der Weijden, C.H., 1999.
626 Weathering, biomass production and groundwater chemistry in an area of dominant anthropogenic
627 influence, the Chaves-Vila Pouca de Aguiar region, north of Portugal. Water, Air Soil Poll. 115(1/4),
628 481−512. doi: 10.1023/A:1005119121666.
629
630 Putnis A., 2002. Mineral replacement reactions: from macroscopic observations to microscopic
631 mechanisms. Mineral. Mag. 66, 689−708. doi: 10.1180/0026461026650056
632
633 Rastogi, B. K., Rao, B. R., Rao, C. V. R. K., 1986. Microearthquake investigations near Sriramsagar
634 Reservoir, Andhra Pradesh State, India. Phys. Earth Planet. Inter. 44, 149–159. doi:10.1016/0031-
635 9201(86)90041-5.
636
637 Roeloffs, E. A., 1997. Poroelastic techniques in the study of earthquake related hydrologic
638 phenomena. Adv. Geophys., 37, 135–195. doi:10.1016/S0065-2687(08)60270-8.
639

640 Sardini, P., Sammartino, S. Tévissen, E., 2001. An image analysis contribution to the study of
641 transport properties of low-permeability crystalline rocks. Comput. Geosci. 27, 1051−1059.
642 doi:10.1016/S0098-3004(00)00157-6 .
643
644 Sausse, J., Jacquot, E., Leroy, J., Lespinasse M., 2001. Evolu tion of crack permeability during fluid–
645 rock interaction. Example of the Brézouard granite (Vosges, France). Tectonophysics 336, 199–214.
646 doi:10.1016/S0040-1951(01)00102-0.
647
648 Shapiro, S. A., Huenges, E., Borm, G., 1997. Estimating the crust permeability
649 from fluid-injection-induced seismicity emission at the KTB site. Geophys. J. Int. 131, F15–F18. doi:
650 10.1111/j.1365-246X.1997.tb01215.x
651
652 Siddiqui, S.H., Parizek, R.R., 1971. Hydrogeologic factors influencing well yields in folded and
653 faulted carbonate rocks in central Pennsylvania. Water Resour. Res. 7(5), 295−1312.
654
655 Talwani, P., 1981. Hydraulic diffusivity and reservoir induced seismicity. Final Tech. Rep., U.S.
656 Geol. Surv., Reston, Va, 48 p.
657
658 Talwani, P., Acree, S., 1984. Pore pressure diffusion and the mechanism of reservoir induced
659 seismicity. Pure Appl. Geophys. 122, 947–965. doi: 10.1007/BF00876395.
660
661 Talwani, P., Cobb, J., 1997. Induced seismicity studies at Bad Creek Reservoir, South Carolina. Final
662 Tech. Rep., U.S. Geol. Surv., Reston, Va, 89 p.
663
664 Van der Weijden, C.H., Pacheco, F.A.L., 2006. Hydrogeochemistry in the Vouga River basin (central
665 Portugal): pollution and chemical weathering. Appl. Geochem. 21, 580–613.
666 doi:10.1016/j.apgeochem.2005.12.006.

667 Verweij, J.M., 1995. Analysis of Pumping Test Data from Hard Rock Aquifers. TNO Report, Institute
668 of Applied Geoscience, England, v. GG R-95-39(A), 65 p.
669
670 White, A.F., Brantley, S.L., 2003. The effect of time on the weathering of silicate minerals: why do
671 weathering rates differ in the laboratory and field? Chem. Geol. 202, 479–506.
672 doi:10.1016/j.chemgeo.2003.03.001.
673
674 Wright, E.P., Burgess, W.D. (1992). The Hydrology of Crystalline Basement Aquifers in Africa.
675 Special Publication 66, Geological Society, London. 264 p. doi: 10.1144/GSL.SP.1992.066.01.01.

WEATHERING OF PLAGIOCLASE ACROSS VARIABLE FLOW AND SOLUTE TRANSPORT REGIMES

Fernando A. L. Pacheco,[a]

Department of Geology & Centre for Chemistry,

Trás-os-Montes and Alto Douro University, Ap 1013, 5000 Vila Real

Portugal

Cornelis H. Van der Weijden,[b]

Department of Earth Sciences—Geochemistry, Faculty of Geosciences,

Utrecht University, P.O. Box 80.021 3508 TA Utrecht,

The Netherlands

Key-words: gravity flow fracture, capillary flow microfracture, advective transport, diffusive transport, open system, semi-open system, weathering, plagioclase, hydraulic diffusivity.

[a] Corresponding author, e-mail FPACHECO@UTAD.PT, Fax. +351 259 350480
[b] e-mail CHVDW@GEO.UU.NL, Fax +31 30 2535302

Abstract

The study area is situated in a fault zone with fractured granites and metassediments. In a conceptual model, infiltrating water first passes the bedrock cover of soil and saprolite and then partly enters the fractures. Weathering reactions of minerals occur in small pores and fissures in the bedrock cover zone to continue in the larger fractures. Pumping tests were carried out in a number of boreholes to measure the drawdown as a function of pumping time. From the results, values of transmissivity (T) could be derived. In combination with the storage coefficient (S) for similar fault zones, the hydraulic diffusivity ($D = T/S$) could be computed.

Water samples, collected from the boreholes, represent fluid packets with a history of weathering reactions in the bedrock cover and in the larger fractures. The major element composition of these samples was used by means of the SiB mass balance algorithm (Pacheco and Van der Weijden, 1996) to calculate the moles·L^{-1} of dissolved plagioclase (oligoclase with An ≈ 0.20) and the moles·L^{-1} of secondary phases (gibbsite, halloysite, smectite) precipitated along the flow paths of the samples. These results were then used to calculate the net dissolved silica concentrations ($[H_4SiO_4^0]$) related to dissolution of plagioclase followed by precipitation of each of the secondary phases. An interpretation of a plot of each of these $[H_4SiO_4^0]$'s versus D is that at $D < 0.7$ m^2·s^{-1}, dissolution of plagioclase is followed by precipitation of halloysite in the large fractures of the fault zone (open system), whereas at $D \geq 0.7$ m^2·s^{-1} precipitation of both halloysite and smectite occurs in the rock matrix with small fissures and pores (semi-open system). Before being pumped, the percolating fluids travelled 0.01 to 13.7 years. During these periods, plagioclase weathered at rates (W_{Pl}) of $10^{-(12.9\pm1.1)}$ moles·m^{-2}·s^{-1}, which are approximately 2.2 orders of magnitude higher than solid-state weathering rates reported in various field studies. In this study, it is

43 suggested that part of the apparent discrepancy between the results is due to changes in
44 hydraulic diffusivity of the weathering environments occurring over the geologic times.
45
46

47 *1. Introduction*

48

49 Weathering of rock forming minerals can be investigated in terms of microsystems, a concept
50 introduced by Korzhinskii (1959). These systems are located at each water–mineral contact
51 and are composed of the primary and secondary minerals and local solutions. They belong to
52 three categories: closed, semi-open and completely open (Meunier et al., 2007). In crystalline
53 rocks, closed microsystems are located at primary porosity and microfracture dead ends,
54 semi-open at microfractures and completely open at small fractures.
55 Groundwater flow and solute transport regimes within a microsystem depend on their
56 category: in a closed system, fluids are stagnant and therefore solute transport is limited; in a
57 semi-open system, water moves by capillarity and solute transport occurs by chemical
58 diffusion; and finally, in an open system, groundwater flow is controlled by gravity and
59 solute transport occurs by advection. The prevailing regimes determine the secondary
60 products derived from alteration of the parent minerals (Baynes and Dearman, 1978; Sausse
61 et al., 2001): in microfractures, where the leaching of solutes is less intense because transport
62 is associated to chemical gradients, the most common secondary products are smectites and
63 vermiculites; in fractures the leaching is intensified because solutes are carried away by the
64 flowing water and, as a consequence allophone and/or halloysite are formed; if velocity
65 and(or) the volume of flow increase, the leaching of (earth)alkaline elements and silica may
66 become extreme, resulting in formation of gibbsite.
67 Dissolution of parent minerals and precipitation of secondary products within microsystems
68 is accompanied by the alteration of rock porosity and permeability. In the process of chemical
69 weathering, water increasingly invades the microsystems developing secondary porosity that,
70 regardless of the quantities of the newly formed phases, generally increases because the
71 alteration products never completely replace the dissolved volume (Putnis, 2002; Meunier et

al., 2007). The increase in porosity changes the geometrical parameters of the pathways. Microfractures tend to widen and connect to other microsystems, increasing permeability (Sardini et al., 2001; Sausse et al., 2001). In later stages of weathering, associated to the development of saprolites, the microstructure of the rocks tends to disappear by collapsing or sliding under gravity, causing a substantial decrease in permeability, but not in porosity (Wright and Burgess, 1992).

Weathering studies based on the microsystem concept have been performed at the microscopic scale (Meunier and Velde, 1979; Hochella and Banfield, 1995; Sausse et al, 2001; Meunier et al., 2007), using thin sections of rock samples as investigating materials.

The main goal of this paper is to extrapolate the analysis of microsystems to the macroscopic scale, applying it to fault zones underlying a soil plus saprolite cover. The selection of fault zones to study the macroscopic behaviour of microsystems is adequate, because fault zones are complex fractured environments composed of large gravity-flow fractures in hydraulic connection with a network of small gravity-flow fractures and capillary-flow microfractures (rock matrix). At the scale of a fault zone, the evolution of pathway parameters can be described by hydraulic diffusivity, which is the ratio of hydraulic transmissivity (a proportion of permeability) to the storage capacity (a function of porosity). The aim is to verify if changes in the hydraulic diffusivity have an effect on the type of secondary minerals formed by weathering of plagioclase.

A complementary objective of this study is to calculate plagioclase weathering rates, taking into account particularities of the fractured rocks relative to groundwater travel time and area exposed to groundwater. The aim is to verify if the relation between weathering rates and groundwater travel time can also be described in terms of progressive hydraulic diffusivity changes.

2. Study Area

The region of Vila Pouca de Aguiar is located in the North of Portugal and occupies an area of approximately 437 km^2 (Figure 1). It is characterized morphologically by large-scale tectonic valleys, associated to the so-called Vila Real fault, surrounded by the Alvão (to the West) and Padrela (to the East) mountains. Altitudes range from a minimum of 200 m in the Northern valleys and a maximum of 1200 m up in the mountains.

Climate in the area is temperate with wet–cold and dry–warm alternating seasons. The annual precipitations range from 900 $mm \cdot yr^{-1}$ in the Northeast to 1900 $mm \cdot yr^{-1}$ in the Southwest of the region (Figure 2), being influenced by the topography.

The geology of the area is characterized by Hercynian (syn- to post-tectonic) granites that intruded Palaeozoic (Cambrian to Devonian) metassediments and were covered by Quaternary alluvial and terrace deposits along the Vila Real fault (Figure 2). In the Southeast part of the area, occupied by an extensive outcrop of metassediments, a geological structure was defined, in which tectonic laminae are folded and separated by major thrusts (Pacheco et al., 1997).

The Vila Pouca de Aguiar granites are composed of (in weight %) quartz (31.5), plagioclase (35.3), K-feldspar (26.7), biotite (4.4) and muscovite (1.4), with minor amounts of apatite and ilmenite. The plagioclase composition ranges from albite-An_8 to andesine-An_{37} (Pacheco et al., 1999). The metassediments, which include greywackes, phyllites, quartzites and graphitic slates, contain quartz, muscovite and smaller amounts of biotite, K-feldspar and albite-oligoclase (Pacheco, 1995).

121 *3. Hydrogeologic Setting*

122

123 *3.1. Conceptual Flow and Weathering Models*

124 The fate of infiltrated rainwater in a fractured massif comprises lateral flow through the
125 bedrock cover (soil and saprolite) and recharge. Recharge includes refilling of the rock
126 matrix, composed of a network of small gravity flow fractures and capillary flow
127 microfractures, and of fault zones composed of large gravity-flow fractures and crushed rock.
128 Figure 3 illustrates the lateral flow of shallow groundwater through a saprolite horizon with a
129 thickness z_0 (m), succeeded by its infiltration into a couple of sub-vertical fault zones. It also
130 shows paths of groundwater through the rock matrix until they reach the same fault zones.
131 Similar models of groundwater flow through fractured rocks towards fault zones have been
132 adopted by Herbert et al. (1992) and Verweij (1995).
133 The saprolite horizon is assumed an open system given the high effective porosity and
134 sometimes (granite saprolites) also high hydraulic conductivity of the disaggregated
135 materials. Depending on precipitation (P, mm), which determines the volume of flow,
136 secondary products expected to result from weathering of plagioclase are halloysite (lower
137 precipitations) or gibbsite (higher precipitations). In Portugal, gibbsite is the most common
138 secondary product for annual precipitations higher than about 1000 $mm \cdot y^{-1}$, whereas for
139 precipitations lower than this limit the dominant product is halloysite (Martins et al., 1995).
140 The fault zones are also assumed open systems because large gravity-flow fractures dominate
141 in these environments. However, no extreme flushing conditions are expected to occur given
142 the compaction of these zones caused by the burden of overlying rocks. For that reason,
143 plagioclase weathering is expected to produce halloysite. Finally, the rock matrix is assumed
144 a semi-open system given the dominance of small gravity-flow fractures and capillary-flow

145 microfractures in this environment. In this case, halloysite and smectite are both assumed
146 products of plagioclase weathering (Meunier et al., 2007).
147
148 *3.2. Boreholes*
149 In the past three decades, about 50 to 60 wells were drilled in the region of Vila Pouca de
150 Aguiar to be used as sources of drinking water for public supply. The location of 31 of the
151 most productive boreholes is plotted in Figure 1 (labelled circles) and the information on
152 name (Id), intersected rock type (granite or metassediment), depth (z, m), slope of the
153 topographic surface (d in %, sampled from the Digital Elevation Model of Figure 1) and local
154 precipitation (P in $mm \cdot y^{-1}$, sampled from Figure 2), is depicted in Table 1. The associated
155 yields are illustrated in Figure 2 and can be justified by a combination of factors
156 encompassing the high annual precipitation, the abundance of quartzites within the
157 metassediments, and especially the proximity of the borehole to the Vila Real fault, to folds
158 and thrusts, or to the contact between granites and metamorphic rocks, places where the
159 fracture sets are usually more dense and interconnected. A number of studies reported the
160 proximity of boreholes to densely fractured regions as an important cause for observed high
161 yields (Siddiqui and Parizek, 1971; Mabee, 1999; Neves and Morales, 2007; among others).
162 During the drillings, several gravity-flow fractures were intersected by the boreholes
163 releasing variable amounts of water. The depth of intersection of fracture i (z_i, m) and its
164 corresponding yield (Q_i, $m^3 \cdot h^{-1}$) are listed in Table 1 for the above mentioned 31 boreholes.
165 Depths of intersection and yields were reported by the well drillers. For the first fracture, the
166 depth was set when water started flowing upward through the borehole emerging naturally at
167 the surface. For the other fractures of the same borehole, depths were set when an increase in
168 the natural outflow was noted. Yields were determined as the rate of water that can be
169 airlifted on a continuous short-term (generally tens of minutes) basis. These approaches for

estimating fractured aquifer depths and yields are common and have been used in many other studies (e.g., Moore et al., 2002). The average depth of the gravity flow fractures (z_{med}, m) was estimated by weighting the depth of each fracture according to its yield:

$$z_{med} = \frac{\Sigma_{j=1}^{n} z_j Q_j}{\Sigma_{j=1}^{n} Q_j} \quad (1)$$

where n is the number of fractures intersected by the borehole.

3.3. Pumping Tests and Hydraulic Parameters

Pumping tests were conducted on 14 of the 31 boreholes, lasting in all cases but one from 1140 to 2760 minutes. The exception was the test conducted on borehole Nr ~~23~~ 22 (Cevivas) which ran for just 330 minutes. The duration of the tests and their pumping rates and hydrostatic levels are listed in Table 2.

In all cases, the scatter points drawdown (s, m) *versus* time (t, min) in a semilogarithmic plot could be fitted with a straight line, after the first 100 minutes of pumping. In three cases (tests to boreholes Nr 4, ~~18~~ 19 and ~~19~~20), the points could be linearly fitted with different two slopes, the first after 10 minutes of pumping and the second after 100 minutes of pumping. Figure 4 illustrates the test to borehole Nr 4. The fitting of (s,t) points to one straight line in a semilogarithmic plot is conform with type curves derived for porous media aquifers, and for that reason aquifer transmissivities (T, $m^2 \cdot s^{-1}$) based on the straight lines fitted to the after-10 and/or after-100 minutes period(s) were calculated using a classical porous media model (the Cooper-Jacob, 1946, formula):

$$T = \frac{2.3Q}{4\pi\Delta s} \quad (2)$$

where Q ($m^3 \cdot s^{-1}$) is the pumping rate and Δs (m) the change in s corresponding to a log cycle of time. The two fittings reported for boreholes Nr 4, 19 and 20 can be attributed to heterogeneity of the tested rocks: boreholes drain several gravity-flow fractures, with

194 different hydraulic heads, that apparently reacted to pumping at two different moments
195 during the test. The influence of rock heterogeneity on pumping test results and interpretation
196 has been quoted by Dagan (1986), Newman (1990), Belcher et al. (2001), Kollet and Zlotnik
197 (2005), among other workers.
198 The hydraulic diffusivity (D, $m^2 \cdot s^{-1}$) is the quotient of transmissivity (T, $m^2 \cdot s^{-1}$) and storage
199 coefficient (S, dimensionless):
200 $$D = T/S \quad (3)$$
201 Fractured rocks and regoliths derived therefrom span a wide range of D values, as depicted in
202 Table 3. The hydraulic conductivity (K, $m \cdot s^{-1}$) is the quotient of transmissivity and the
203 drainable thickness (b, m):
204 $$K = T/b \quad (4)$$
205 The drained thicknesses of the tested boreholes are listed in Table 2 and were estimated by
206 multiplying the number of intersected fractures (Table 1) by the length of the screened tubes
207 casing the borehole around those fractures (in general 6 m, but 3 or 1 m for boreholes
208 Cevivas and Santa Marta, respectively). Effective porosity (n_e, dimensionless) is the volume
209 of connected voids in a sample divided by the total volume of the sample, and can be derived
210 from the storage coefficient (Domenico and Schwartz, 1998):
211 $$n_e = \frac{S}{\rho_w b \sigma_w} \quad (5)$$
212 where ρ_w is the specific weight of water (999.1 $kg \cdot m^{-3}$ at T = 15ºC) and σ_w the
213 compressibility coefficient of water (4.7×10^{-9} $m^2 \cdot kg^{-1}$).
214 *4. Sampling and Analysis*Samples of borehole water were collected within the limits of the
215 Vila Pouca de Aguiar municipality from January 2006 to April 2006. The sampling sites are
216 shown in Figure 1. At the sampling site, electrical conductivity (EC), temperature (T, ºC) and
217 pH were measured and a water sample was filtered through a 0.4 μm membrane filter. The

filtered water was split into 2 portions; one was stored for analysis in the home laboratory, acidified to pH 2 using pure nitric acid, and the other for analysis of alkalinity in the field laboratory, within 24 hours using the Gran plot method. In the home laboratory, ICP-OES was used for analysis of Si. The analytical results are shown in Table 4.

5. Weathering Reactions and Rates

Not all minerals present in the granites or in the metassediments are important as weathering reactants. In general, the abundance of plagioclase in granites is significant and therefore the relative contribution of plagioclase weathering to groundwater composition is expected to be expressive. However, because plagioclase has a low resistance to weathering, when compared to other minerals composing these rocks (e.g. quartz, biotite, muscovite; Bland and Rolls, 1998; Appelo and Postma, 2005), this relative contribution may not be just expressive but dominant. For example, in granite areas of central Portugal, Pacheco and Van der Weijden (1996) and Van der Weijden and Pacheco (2006) reported contributions greater than 90%. In the Vila Pouca de Aguiar granites, this dominance was also recognised by Pacheco et al. (1999), which reported contributions between 95 and 98%, and of 99% when weathering was associated to fault zones. In the metassediments, plagioclase may be present solely in small amounts. However, weathering of plagioclase may also contribute dominantly to ground water composition, because the surrounding minerals (e.g. quartz, chlorite) are usually much less reactive. For example, in an area with metassediments where groundwater chemistry was explained by weathering of plagioclase (albite) and chlorite (Pacheco and Alencoão, 2006), the abundance of chlorite is about twice the abundance of albite, but on average the relative contribution of albite weathering to groundwater composition is greater than 90%. For the

242 reasons described above, it is assumed in this case that plagioclase weathering explains the
243 natural composition of ground water, namely the concentrations of silica and bicarbonate.
244
245 *5.1. Mass Balances*
246 Reactions of plagioclase producing gibbsite, halloysite, or smectite are listed in Table 5. The
247 contribution of each reaction to groundwater composition can be accomplished by solving a
248 set of mole balance equations based on the reaction stoichiometries, namely on the
249 bicarbonate to dissolved silica ratio (*r*) which is a key parameter in distinguishing between
250 different reactions (Garrels, 1967; Pacheco and Van der Weijden, 1996). For the reactions
251 listed in Table 5, the ratios are:

252 $$r_{\mathrm{Gibb}} = \frac{1+x}{3-x} \quad (6a)$$

253 $$r_{\mathrm{Hal}} = \frac{1}{2}\frac{1+x}{1-x} \quad (6b)$$

254 $$r_{\mathrm{Sm}} = \frac{0.6(1+x)}{0.95-5.65x} \quad (6c)$$

255 where x is the anorthite content of plagioclase ($0 \le x \le 1$), and the mole balance equations
256 are:

257 $$\left[HCO_3^-\right] = r_{\mathrm{Gibb}}[H_4SiO_4^0]_{\mathrm{Gibb}} + r_{\mathrm{Hal}}[H_4SiO_4^0]_{\mathrm{Hal}} + r_{\mathrm{Sm}}[H_4SiO_4^0]_{\mathrm{Sm}} \quad (7a)$$

258 $$[H_4SiO_4^0] = [H_4SiO_4^0]_{\mathrm{Gibb}} + [H_4SiO_4^0]_{\mathrm{Hal}} + [H_4SiO_4^0]_{\mathrm{Sm}} \quad (7b)$$

259 where square brackets represent dissolved concentrations. The unknowns of the system are x
260 and the partial concentrations of dissolved silica. An average value for x can be obtained
261 from chemical analysis of granite and metassediment plagioclases (in the Vila Pouca de
262 Aguiar region, plagioclase is faithfully represented by an oligoclase, meaning that $x \approx 0.2$).
263 However, to become a determined system, set 7a,b must be completed with an additional
264 equation.

According to the conceptual flow and weathering models illustrated in Figure 3, the concentration derived from reaction R_{Gibb} ($[H_4SiO_4^0]_{Gibb}$) is released when shallow groundwater moves along the saprolite path, whereas the concentrations derived from R_{Hal} ($[H_4SiO_4^0]_{Hal}$) and R_{Sm} ($[H_4SiO_4^0]_{Sm}$) are released or consumed along the fault zone plus rock matrix paths. In the first case, the movement of water is sideways and water-mineral interactions occur within a relatively narrow depth range (from ground surface to z_0). Solute concentrations will be higher or lower depending on whether the length of the saprolite flow path is longer (*lsp* in Figure 3) or shorter (*ssp*), but they will be independent of circulation depth (z). In the second case, water moves laterally as well as vertically, being sampled in the boreholes at a depth $z = z_{med}$. The value of z_{med} varies from place to place (e.g., from 18 to 96 meters in the study area, Table 1). If dissolution of plagioclase and transport of silica along the fault zone plus rock matrix paths are assumed continuous, then a range in circulation depths are expected to follow a concomitant range in the dissolved silica concentrations, the overall result being a regression between $[H_4SiO_4^0]_{Hal} + [H_4SiO_4^0]_{Sm}$ and z_{med}. This relationship is not universal but can be defined for each particular case. With this relation added to Equations 7a,b, the set becomes determined, and a unique solution can be found for its unknowns.

5.2. Moles of Dissolved Plagioclase

The moles of plagioclase ([Pl]) dissolved along the saprolite, fault zone and rock matrix flow paths are obtained by multiplying the concentrations of silica derived from reactions R_{Gibb}, R_{Hal} and R_{Sm} by the concomitant plagioclase to silica ratios (β), as deduced from Table 5:

$$[Pl] = \beta_{Gibb}[H_4SiO_4^0]_{Gibb} + \beta_{Hal}[H_4SiO_4^0]_{Hal} + \beta_{Sm}[H_4SiO_4^0]_{Sm} \quad (8)$$

where

$$\beta_{Gibb} = \frac{1}{3-x} \quad (9a)$$

290 $$\beta_{Hal} = \frac{1}{2(1-x)} \quad (9b)$$

291 $$\beta_{Sm} = \frac{1.65}{0.95-5.65x} \quad (9c)$$

292 The first term of the right-hand side of Equation 8 represents the number of moles of
293 plagioclase dissolved along the saprolite path ($[Pl]_0$) whereas the sum of the second and third
294 terms represent the moles dissolved along the fault zone plus rock matrix paths.

295

296 *5.3. Plagioclase Weathering Rates*

297 Weathering rates of plagioclase can be estimated using:

298 $$W_{Pl} = \frac{[Pl]-[Pl]_0}{t} \times \frac{V_r}{A_{Pl}} \quad (10)$$

299 where W_{Pl} ($mol \cdot m^{-2} \cdot s^{-1}$) is the rate and $[Pl]-[Pl]_0$ ($mol \cdot m^{-3}$) its concomitant dissolved
300 concentration, t (s) is the average groundwater travel time of water packets flowing through
301 the fault zone and through the rock matrix, V_r ($m^3 \cdot s^{-1}$) is the volume of water entering the
302 fault zone in a unit time, and A_{Pl} ($m^2 \cdot s^{-1}$) is the surface area of plagioclase in contact with that
303 volume of aquifer water. An equation for A_{Pl} was developed by Pacheco and Alencoão
304 (2006), describing the area of fracture surfaces in contact with aquifer water in unit time:

305 $$A_{Pl} = 2\alpha_{Pl} V_r \times \sqrt{\frac{\rho_w g n_e}{12 \mu_w K}} \quad (11)$$

306 where α_{Pl} is the proportion of plagioclase in the rock, μ_w (1.14×10^{-3} $kg \cdot s^{-1} \cdot m^{-1}$ at T = 15ºC)
307 is the dynamic viscosity of water, and g is the acceleration of gravity (9.81 $m \cdot s^{-2}$). Replacing
308 this equation in Equation 10 and rearranging gives:

309 $$W_{Pl} = \frac{[Pl]-[Pl]_0}{2t\alpha_{Pl}} \sqrt{\frac{12\mu_w K}{\rho_w g n_e}} \quad (12a)$$

310 Further substitution of Equation 5 in Equation 12a gives

311 $$W_{Pl} = \frac{[Pl]-[Pl]_0}{2t\alpha_{Pl}} C_w \sqrt{D} \quad (12b)$$

where

$$C_w = \sqrt{\frac{12\mu_w\sigma_w}{g}} = 2.56\times10^{-6}\ \text{s}^{1/2}\ (\text{at } T = 15^{\circ}\text{C}) \quad (12c)$$

Equation 12b describes the weathering rate as an explicit function of hydraulic diffusivity.

6. Groundwater Travel Times

The average groundwater travel time is the length of the flow path divided by the mean velocity of water along that path. According to the conceptual flow model (Figure 3), water will move towards the fault zones following two distinct paths: the fault zone path or the rock matrix path. The length of the fault zone path can be equated to $z_{med}-z_0$, assuming that fault zones are almost vertical, where z_{med} is the average depth to the conductive fractures (Equation 1) and z_0 is the thickness of the saprolite layer. The length of the rock matrix path is difficult to assess, because it depends on the average distance between the recharge areas and the fault zones as well as on the tortuosity of the path, which are unknowns. In this study, the length of the flow path was approached to $z_{med}-z_0$. This provides minimum values for flow path lengths and consequently to groundwater travel times, maximizing weathering rates (Equation 12). Difficulties in determining the rock matrix flow path length were also encountered and not resolved by Meunier et al. (2007). The mean velocity of water along the flow path (v, $\text{m}\cdot\text{s}^{-1}$) is (Domenico and Schwartz, 1998):

$$v = \frac{Ki}{n_e} \quad (13)$$

where i is the hydraulic gradient (dimensionless). Although hydraulic gradients are influenced by recharge and discharge rates as well as by groundwater withdrawal, they follow primarily the local relief (Appelo and Postma, 2005), being determined by the slope of the topographic surface (d, dimensionless). Hence, the travel time of groundwater moving from

the bottom of the saprolite layer till the average depth of conductive fractures can be written as:

$$t = \frac{(z_{med} - z_0)n_e}{Kd} \quad (14)$$

It should be mentioned that K and n_e were estimated from results of long-term pumping tests, and therefore correspond to an average of the hydraulic conductivities and effective porosities of the fault zone plus rock matrix.

7. Results and Discussion

7.1. Hydraulic Tests

The hydraulic test of borehole Bornes 1 (Figure 4) ran at a pumping rate $Q = 13.5\times10^{-3}$ $m^3 \cdot h^{-1}$ (Table 2). For the log cycle 10 to 100 minutes, the scatter points fit to a straight line with drawdowns $s_{10} = 2.5$ and $s_{100} = 7.8$ m, respectively. The change in the drawdown is $\Delta s_1 = 5.3$ m which results in $T_1 = 1.31\times10^{-4}$ $m^2 \cdot s^{-1}$ (Equation 2). For the next log cycle of time (100 to 1000 minutes) the scatter points fit to a less inclined straight line resulting in a smaller $\Delta s_2 = 2.3$ m and a larger transmissivity $T_2 = 3.05\times10^{-4}$ $m^2 \cdot s^{-1}$. Even though the time spans linked to T_1 and T_2 are usually different (Figure 4), the average fault zone transmissivities were calculated using the arithmetic mean $(T_1+T_2)/2$. For the fault zone intersected by borehole Bornes 1, $T_{med} = 2.18\times10^{-4}$ $m^2 \cdot s^{-1}$. When considering the results of all pumping tests, $T_{med} = (1.5\pm1.2)\times10^{-4}$ $m^2 \cdot s^{-1}$. There were no observation wells around the tested boreholes so a reasonable value had to be found for the storage coefficient. The choice was the average storage coefficient of a 33.2 m thick fault zone estimated by Pacheco (2002): $S = (7.75\pm1.71)\times10^{-5}$. Standing on this coefficient, the hydraulic diffusivities were calculated by Equation 3 and compiled in Table 4. On average, $D = 1.7\pm1.4$ $m^2 \cdot s^{-1}$. These values lie in a range of values observed for fractured weathered crystalline rocks (0.1–10 $m^2 \cdot s^{-1}$; Table 3)

and are in agreement with results obtained in other studies (Talwani, 1981; Talwani and Acree, 1984; Rastogi et al., 1986; Shapiro et al, 1997; Talwani and Cobb, 1999).

For borehole Bornes 1, b = 18 m and so $K_{med} = 12.1\times10^{-6}\ m\cdot s^{-1}$ (Equation 4). For the entire set of tested wells $K_{med} = (8.8\pm5.7)\times10^{-6}\ m\cdot s^{-1}$ (Table 2). Hydraulic conductivities decrease steadily with z_{med} as shown in Figure 5. The scatter points in this figure can be fitted to an exponential function:

$$K(\times10^{-6}\,m\cdot s^{-1}) = 53.37e^{-0.051z_{med}},\ R^2 = 0.7 \quad (15)$$

This equation was used to estimate hydraulic conductivities for the non-tested boreholes (Table 4). The effective porosity was based on the adopted storage coefficient ($S = 7.75\times10^{-5}$), and was estimated using Equation 5. The result was: $n_e = 0.50$.

7.2. Weathering Reactions

The physicochemical parameters of the sampled waters are given in Table 4. During the saprolite, fault zone and rock matrix paths, reaction of water with rock forming minerals releases solutes and precipitates clay minerals, hydroxides, etc. One of the reaction-derived solutes is silica ($H_4SiO_4^0$) and for the studied borehole waters the concentrations of $H_4SiO_4^0$ ($mol\cdot L^{-1}$) increase with depth (z_{med}, Figure 6). The sympathy between $[H_4SiO_4^0]$ and z_{med} is clear, in spite of the scatter bounded by two dashed lines. This scatter can be ascribed to the contribution of saprolite weathering to $[H_4SiO_4^0]$, i.e. to weathering occurring before the entrance of shallow ground water into the rock matrix and fault zones intersected by the drilled wells, because this contribution is not supposed to depend on z_{med}. According to the conceptual weathering model described before, the saprolite contribution to weathering is referred to as $[H_4SiO_4^0]_{Gibb}$. Since water moves laterally along the saprolite path (Figure 3), interacting with minerals within a narrow range of circulation depths (0–z_0 meters), there is

no reason why $[H_4SiO_4^0]_{Gibb}$ should depend on z_{med}. Instead, $[H_4SiO_4^0]_{Gibb}$ should vary in agreement with changes in the saprolite path length, as interpreted from a detailed analysis of Figure 6. In this figure, we shall presume that $[H_4SiO_4^0]_{Gibb}$ is represented by a point in the dotted line. This line marks the intersection between the lower dashed line and the X-axis (z_0) and stands for the average thickness of the saprolite layer (z_0 = 16 m). If the path followed by groundwater during the stage of saprolite weathering is the largest (*lsp* in Figure 3) then $[H_4SiO_4^0]_{Gibb}$ is also the largest and represented by the intersection between the upper dashed line and the dotted line. If this path is the shortest (*ssp*) then $[H_4SiO_4^0]_{Gibb}$ will approach zero and be represented by the intersection between the lower dashed line and the dotted line. In general (values in Table 4),

$$[H_4SiO_4^0]_{Gibb} = [H_4SiO_4^0] - 0.0043(z_{med}-z_0) \quad (16)$$

where 0.0043 is the slope of the dashed lines.

For the present case study, Equation 16 is required to convert Equations 7a,b into a set with a unique solution for $[H_4SiO_4^0]_{Hal}$ and $[H_4SiO_4^0]_{Sm}$.

The concentrations of silica derived from reactions R_{Gibb}, R_{Hal} and R_{Sm} (Table 5) are listed in Table 4. In all cases $[H_4SiO_4^0]_{Gibb}$ and $[H_4SiO_4^0]_{Hal}$ are positive, meaning that the corresponding reactions invariably release silica to solution. With four exceptions (samples from drilled wells Nr ~~10~~11, ~~11~~12, ~~16~~ 17 and ~~25~~26), $[H_4SiO_4^0]_{Sm}$ is negative, meaning that R_{Sm} generally consumes silica from solution. These results are in keeping with the equations for the *r* ratios (Equations 6a–c), because for any value of x r_{Gibb} and r_{Hal} are positive while r_{Sm} is positive only for x < 0.056 (albite). The exceptions represent cases where adoption of x = 0.2 is inadequate. For the cases where R_{Sm} consumes silica, the reaction proceeds only if there is some silica available in the solution, for example transported along the flow path from places

where weathering of plagioclase has released this solute, i.e. from places where R_{Gibb} or R_{Hal} were the prevailing reactions.

7.3. Weathering Reactions and Hydraulic Diffusivity

A plot of silica concentrations derived from reactions R_{Hal} and R_{Sm} (Table 5) *versus* hydraulic diffusivity (D) is illustrated in Figure 7. For silica released by R_{Hal}, concentrations decrease as D increases, according to a power function. When silica is consumed by R_{Sm}, this consumption increases for increasing values of D, according to a linear function.

Fault zones are low diffusive environments because water tends to follow large gravity fractures (the easiest routes). Contrarily, the rock matrix is potentially a high diffusive environment because water has to move in a network of connected small gravity flow fractures and capillary flow microfractures; the higher the connectivity the higher the hydraulic diffusivity (Knudby and Carrera, 2006). According to this setting, fault zones must be plotted to the left-hand side of Figure 7 and the rock matrix to the right-hand side of that diagram. The boundary between the two environments must be drawn in keeping with the conceptual weathering model described before. According to this model, reactions involving plagioclase and occurring along fault zones (completely open systems) should be related to precipitation of halloysite, and reactions occurring along the rock matrix (semi-open system) to precipitation of smectite plus halloysite. In Figure 7, this scenario becomes more evident for $D \approx 0.7$ $m^{-2} \cdot s^{-1}$: when $D < 0.7$ $m^{-2} \cdot s^{-1}$, concentrations derived from R_{Hal} are high (average: 280 $mmol \cdot L^{-1}$) and concentrations related to R_{Sm} approach zero (average: −16 $mmol \cdot L^{-1}$); for $D > 0.7$ $m^{-2} \cdot s^{-1}$, both reactions play a role in weathering of plagioclase (the average concentrations are 158 $mmol \cdot L^{-1}$ for R_{hal} and −67 $mmol \cdot L^{-1}$ for R_{sm}), with a growing relative importance of R_{Sm}. Although the limit of $D = 0.7$ $m^{-2} \cdot s^{-1}$ may be considered arbitrary, it

certainly can be used as provisional threshold for the separation between fault zone (open system) and rock matrix (semi-open system) weathering.

An association can also be recognized between precipitation of halloysite and advective flow along gravity fractures of the fault zones and rock matrix. This is illustrated in Figure 8. No correlation exists between $[H_4SiO_4^0]_{Gibb}$ and z_{med}, but even was not expected as production of gibbsite is ascribed to the saprolite path, not to the fault zone or rock matrix paths. A correlation between the remainder of silica ($[H_4SiO_4^0]_{Hal}$ + $[H_4SiO_4^0]_{Sm}$) and z_{med} was already discussed (Figure 6) but Figure 8 shows that only $[H_4SiO_4^0]_{Hal}$ is correlated with depth. This is a remarkable result because confirms that production of halloysite is indeed associated with plagioclase weathering along the mean direction of flow, and that the same does not hold for production of smectite. In keeping with these results, it may be concluded that production of halloysite does occur along the walls of gravity-flow fractures, in fault zones or the rock matrix. In these two media, solute transport is advective and therefore concentrations must increase with increasing flow path lengths (z_{med}) justifying the observed correlation. Conversely, production of smectite occurs at micro fractures adjacent to the gravity flow fractures, where solute transport is diffusive, mediated by local gradients of chemical potential and by the length of diffusion trajectories between the capillary and gravity-flow fractures, and hence not necessarily dependent on the flow path lengths.

7.4. Groundwater Travel Times, Plagioclase Weathering Rates and Hydraulic Diffusivity

Groundwater travel times (t) calculated by Equation 14 are given in Table 4 and range from 0.01 to 13.7 years, being on average 2.2±3.5 yr. Plagioclase weathering rates (W_{Pl}) calculated by Equation 12b are compiled in Table 4, with an average logarithmic value of –12.9±1.1. These rates are plotted in Figure 9 (filled circles) along with field weathering rates reported in

456 other studies (White and Brantley, 2003, and references therein; open circles), with an
457 average logarithmic value of −15.1±1.0.
458 Literature rates are on average 2.2 orders of magnitude lower than the rates calculated in this
459 study. In a first glance at Figure 9, it could be suggested that factor time is the sole
460 explanation for this discrepancy, but a thorough analysis of the various results reveals that
461 other factors are also important. The open circles are mostly solid-state weathering rates
462 based on the differences between elemental, isotopic and mineral compositions measured in
463 present-day regoliths and in the assumed protolith. In these cases, variable *t* represents the
464 entire time span of a weathering episode, commonly on the order of thousands to million
465 years. The filled circles are solute-flux rates that stand for contemporary weathering during
466 groundwater percolation in the fractured rocks, in which case *t* (travel time) is just a portion
467 of that time window, frequently ranging from years to decades. For the open circles, it is
468 inherently assumed that the weathering environment is initially a fresh rock (the protolith),
469 i.e. a medium with a very high hydraulic diffusivity (Table 3). For the filled circles, it is
470 recognised that many groundwater parcels have circulated through the fractured rocks over
471 the full time span of weathering, which had as consequence a progressive decrease in the
472 hydraulic diffusivity, till present day values that do not exceed 5 $m^2 \cdot s^{-1}$ (Table 4).
473 The consequences for weathering rates of changing the hydraulic properties of the percolated
474 rocks are predicted by Equation 12b: the impact in the W_{Pl} values is proportional to the square
475 root of the change in the *D* values. To elucidate the full relationship between weathering rate,
476 hydraulic diffusivity and time, an equation describing the drop in *D* as a function of *t* has to
477 be defined. If, as working hypothesis, it is assumed that *D* decreases according to a power
478 function of *t*, then Equation 12b can be rewritten as:

479 $$W_{Pl} = \frac{[\mathrm{Pl}] - [\mathrm{Pl}]_0}{2(\eta t)\alpha_{\mathrm{Pl}}} C_w \sqrt{D_0 (\eta t)^{-f/\eta}} \qquad (17)$$

480 with t given in years and where f is the decreasing rate, η converts years into seconds (η
481 $=3.1536\times10^{7}$ s·yr^{-1}), and D_0 is a proxy for the initial hydraulic diffusivity. The plot of
482 Equation 17 in Figure 9 is represented by the dotted lines, each one representing a different
483 D_0. In this plot, it is assumed that $[Pl] - [Pl]_0 = 0.686$ mol·m^{-3} (the average value; Table 4),
484 that $\alpha_{Pl} = 0.353$ (the proportion of plagioclase in the granites) and that $f = 1$. According to the
485 distribution of the D_0 lines, most solid-state rates are indeed related to the weathering of a
486 protolith with $10^3 < D_0 < 10^6$ m^2/s whereas solute-flux rates are related to a weathered
487 fractured rock with $10^{-2} < D_0 < 10^2$ m^2/s. It is also clear that, in case the aquifers investigated
488 in this study were composed of average diffusivity protoliths ($D_0 = 10^5$ m^2·s^{-1}; Table 3),
489 instead of being composed of low diffusivity weathered fractured rocks ($D_0 \approx 10^0$ m^2·s^{-1};
490 Table 4), the calculated rates would be 2.5 orders of magnitude higher (A-double arrowed
491 line in Figure 9). This difference may be defined as the impact on weathering rates resulting
492 from continuous recirculation of groundwater through the studied fault zones, over the
493 geologic times. Factor time adds up to the previous impact, being minimal for waters that
494 circulated through the system only a few days or months and maximum for waters with
495 residence times of several years or decades. In the studied region, the difference between
496 minimum and maximum rates spans 4 orders of magnitude (B-double arrowed line). In
497 summary, the past changes in hydraulic diffusivity till present day values account for
498 approximately 40% reduction in weathering rates (2.5 orders of magnitude), relatively to their
499 presumed original values, whereas travel time accounts for the remaining 60% (4 orders).
500
501 *8. Conclusions*
502
503 The drawdown (s) in boreholes (observed during pumping tests), plotted against log cycles of
504 pumping time (t) could be fitted by two straight lines, one for a short (10 to 100 minutes), the

505 other for a longer (100 to 1000 minutes) period of pumping time. Using the latter results, the
506 average transmissivity (T) was estimated and, in combination with an average storage
507 coefficient (S) typical for regional fault zones, the hydraulic diffusivity ($D = T/S$) could be
508 calculated: on average $D = 1.7 \pm 1.4$ $m^2 \cdot s^{-1}$. Lower values of D are typical for fault zones with
509 large fractures, while higher values are indicative of connected networks of small to very
510 small fractures typical for the rock matrix. Applying the so-coined SiB mass balance
511 equations (Pacheco and Van der Weijden, 1996) to the water composition, the contribution of
512 dissolved plagioclase to the water chemistry as well as the amounts of secondary precipitates
513 (gibbsite, halloysite, smectite) withdrawn from these waters can be calculated. Next, the net
514 release of dissolved silica from plagioclase dissolution in combination with precipitation of
515 gibbsite and halloysite and its consumption by smectite formation can be computed. The net
516 release of dissolved silica derived from plagioclase dissolution in combination with halloysite
517 precipitation correlates with the average depth (z_{med}) of the productive sectors of the drilled
518 wells, strongly suggesting halloysite precipitation along fractures in the bedrock.
519 Combinations of dissolved silica concentrations derived from plagioclase dissolution with
520 precipitation of gibbsite or smectite lack a correlation with z_{med}. The relation between the net
521 dissolved silica concentrations and D suggests that for $D < 0.7$ $m^2 \cdot s^{-1}$ the weathering of
522 plagioclase is largely followed by precipitation of halloysite and takes place in the completely
523 open system of the fault zone, whereas at higher values reactions occur also in the rock
524 matrix with precipitation of both halloysite and smectite. Groundwater travel times are on
525 average 2.2±3.5 year. Weathering rates (W_{Pl}*'s*) are calculated from the moles of plagioclase
526 dissolved along the flow path per unit of area of plagioclase exposed to the fluid and travel
527 time t. The average $(W_{Pl}) = 10^{-(12.9 \pm 1.1)}$ $mol \cdot m^2 \cdot s^{-1}$ is 2.2 orders of magnitude higher than
528 solid-state weathering rates reported in various studies. The explanations for the apparent
529 discrepancy are partly the past changes in hydraulic diffusivity of the weathering

530 environments, from approximately 10^5 m^2/s in the protoliths to 0.1–1 m^2/s in present-day
531 weathered fractured rocks, and partly the duration of weathering.
532

533 **References**

534

535 Abrisqueta, J. M., Plana, V., Ruiz-Canales, A., Ruiz-Sánchez, M. C, 2006. Unsaturated hydraulic
536 conductivity of disturbed and undisturbed loam soil. Span. J. Agric. Res. 4(1), 91–96.

537

538 Appelo, C.A.J., Postma, D., 2005. Geochemistry, Groundwater and Pollution. A.A. Balkema,
539 Rotterdam, 649 pp.

540

541 Baynes J., Dearman, W.R., 1978. The microfabric of a chemically weathered granite. Bull. Eng. Geol.
542 Environ.18, 91−100. doi: 10.1007/BF02635354

543

544 Belcher, W.R., Elliott, P.E., Geldon, A.L., 2001. Hydraulic-property estimates for use with a transient
545 ground-water flow model for the Death Valley regional ground-water flow system, Nevada and
546 California: U.S. Geological Survey Water-Resources Investigations Report 01−4210. url:
547 http://water.usgs.gov/pubs/wri/wri014210/.

548

549 Bland, W., Rolls, D., 1998. Weathering: and Introduction to the Scientific Principles. Arnold, London,
550 271p.

551

552 Cooper, H.H., Jacob, C.E., 1946. A generalized graphical method for evaluating the formation
553 constants and summarizing well field history. Transactions American Geophysical Union 27,
554 526−534.

555

556 Dagan, G., 1986. Statistical theory of groundwater flow and transport: Pore to laboratory, laboratory
557 to formation, and formation to regional scale. Water Resour. Res. 22(9), 120S−135S.
558 doi:10.1029/WR022i09Sp0120S

559

560 Domenico, P.A., Schwartz, F.W., 1998. Physical and Chemical Hydrogeology (2nd ed.). John Wiley &
561 Sons Inc., New York, 506pp. doi: wiley.com/ 10.1002/ 1099-1034(200004/ 06)35
562
563 Garrels, R.M., 1967. Genesis of some ground waters from igneous rocks. In: Abelson, P.H. (Ed.),
564 Researches in Geochemistry, Wiley, New York, v. 2, pp. 405–420.
565
566 Herbert, R., Barker, J.A., Kitching, R., 1992. New approaches to pumping test interpretation for dug
567 wells constructed on hard rocks. In: Burgess, E.P. (Ed.), Hydrogeology of crystalline basement
568 aquifers in Africa. Geological Society Special Publication, no. 66, pp. 221–242. doi: 10.1144/
569 GSL.SP.1992.066.01.11.
570
571 Hochella, M.F., Banfield, J.F., 1995. Chemical weathering of silicates in nature: a microscopic
572 perspective with theoretical considerations. In: White, A.F. & Brantley, S.L. (Eds.), Chemical
573 Weathering Rates of Silicate Minerals. Reviews in Mineralogy 31, Mineralogical Society of America,
574 pp. 353–406.
575
576 Knudby, C., Carrera, J., 2006. On the use of apparent hydraulic diffusivity as an indicator of
577 connectivity. J. Hydrol. 329, 377–389. doi:10.1016/j.jhydrol.2006.02.026.
578
579 Kollet, S.J., Zlotnik, V.A., 2005. Influence of aquifer heterogeneity and return flow on pumping test
580 data interpretation. J. Hydrol. 300(1−4), 267–285. doi:10.1016/j.jhydrol.2004.06.011.
581
582 Korzhinskii, D.S., 1959. Physicochemical Basis of the Analysis of the Paragenesis of Minerals
583 (translation). Consultant Bureau, New York, 143 p.
584
585 Mabee, S.B., 1999. Factors influencing well productivity in glaciated metamorphic rocks.
586 Groundwater 37(1), 88–97. doi: 10.1111/j.1745-6584.1999.tb00961.x.

587 Martins, A.A.A., Madeira, M.V., Refega, A.A.G., 1995. Influence of rainfall on properties of soils
588 developed on granite in Portugal. Arid Soil Res. Rehabil. 9, 353–366. doi:
589 10.1080/15324989509385904.
590
591 Meunier, A., Velde, B., 1979. Weathering mineral facies in altered granites: the importance of local
592 small-scale equilibria. Mineral. Mag, 43, 261–268.
593
594 Meunier, A., Sardini, P., Robinet, J.C., Prêt, D., 2007. The petrography of weathering processes: facts
595 and outlooks. Clay Miner. 42, 415–435. doi: 10.1180/claymin.2007.042.4.01
596
597 Moore, R.B., Schwarz, G.E., Clark Jr., S. F., Walsh, G.J., Degnan, J. R., 2002. Factors Related to
598 Well Yield in the Fractured-Bedrock Aquifer of New Hampshire. U.S. Geol. Survey Prof. Paper 1660,
599 22p.
600
601 Neuman, S.P., 1975. Analysis of pumping test data from anisotropic unconfined aquifers considering
602 delayed gravity response. Water Resour. Res. 11(2), 329–342.
603
604 Neves, M.A., Morales, N., 2007. Structural control over well productivity in the Jundiaí River
605 Catchment, Southeastern Brazil. Annals of the Brazilian Academy of Sciences 79(2), 307–320.
606
607 Pacheco, F.A.L., 1995. Interacção Água-Rocha em Unidades do Grupo Peritransmontano (Serra da
608 Padrela-Vila Pouca de Aguiar). MSc Thesis, Coimbra University, Coimbra, 123p.
609
610 Pacheco, F.A.L., 2002. Response to pumping of wells in slopping fault-zone aquifers. J. Hydrol.
611 259(1–4), 116–135. doi: 10.1016/S0022-1694(01)00584-4
612

613 Pacheco, F.A.L., Alencoão, A.M.P., 2006. Role of fractures in weathering of solid rocks: narrowing
614 the gap between experimental and natural weathering rates. J. Hydrol. 316, 248–265.
615 doi:10.1016/j.jhydrol.2005.05.003.
616
617 Pacheco, F.A.L., and Van der Weijden, C.H., 1996. Contributions of water-rock interactions to the
618 composition of groundwater in areas with a sizable anthropogenic input. A case study of the waters of
619 the Fundão area, central Portugal. Water Resour. Res. 32(12), 3553–3570. doi:10.1029/96WR01683.
620
621 Pacheco, F.A.L., Sousa, L.M.O., Sousa Oliveira, A., 1997. The Supply of a Small Town with
622 Groundwater from Thrusted Quartzites. In: Marinos, P.G. et al. (eds.), Engineering Geology and the
623 Environment, Balkema, Rotterdam, v. 2, pP. 1407−1412.
624
625 Pacheco, F.A.L., Sousa Oliveira, A., Van der Weijden, A.J., Van der Weijden, C.H., 1999.
626 Weathering, biomass production and groundwater chemistry in an area of dominant anthropogenic
627 influence, the Chaves-Vila Pouca de Aguiar region, north of Portugal. Water, Air Soil Poll. 115(1/4),
628 481−512. doi: 10.1023/A:1005119121666.
629
630 Putnis A., 2002. Mineral replacement reactions: from macroscopic observations to microscopic
631 mechanisms. Mineral. Mag. 66, 689−708. doi: 10.1180/0026461026650056
632
633 Rastogi, B. K., Rao, B. R., Rao, C. V. R. K., 1986. Microearthquake investigations near Sriramsagar
634 Reservoir, Andhra Pradesh State, India. Phys. Earth Planet. Inter. 44, 149–159. doi:10.1016/0031-
635 9201(86)90041-5.
636
637 Roeloffs, E. A., 1997. Poroelastic techniques in the study of earthquake related hydrologic
638 phenomena. Adv. Geophys., 37, 135–195. doi:10.1016/S0065-2687(08)60270-8.
639

640 Sardini, P., Sammartino, S. Tévissen, E., 2001. An image analysis contribution to the study of
641 transport properties of low-permeability crystalline rocks. Comput. Geosci. 27, 1051−1059.
642 doi:10.1016/S0098-3004(00)00157-6 .
643
644 Sausse, J., Jacquot, E., Leroy, J., Lespinasse M., 2001. Evolu tion of crack permeability during fluid–
645 rock interaction. Example of the Brézouard granite (Vosges, France). Tectonophysics 336, 199–214.
646 doi:10.1016/S0040-1951(01)00102-0.
647
648 Shapiro, S. A., Huenges, E., Borm, G., 1997. Estimating the crust permeability
649 from fluid-injection-induced seismicity emission at the KTB site. Geophys. J. Int. 131, F15–F18. doi:
650 10.1111/j.1365-246X.1997.tb01215.x
651
652 Siddiqui, S.H., Parizek, R.R., 1971. Hydrogeologic factors influencing well yields in folded and
653 faulted carbonate rocks in central Pennsylvania. Water Resour. Res. 7(5), 295−1312.
654
655 Talwani, P., 1981. Hydraulic diffusivity and reservoir induced seismicity. Final Tech. Rep., U.S.
656 Geol. Surv., Reston, Va, 48 p.
657
658 Talwani, P., Acree, S., 1984. Pore pressure diffusion and the mechanism of reservoir induced
659 seismicity. Pure Appl. Geophys. 122, 947–965. doi: 10.1007/BF00876395.
660
661 Talwani, P., Cobb, J., 1997. Induced seismicity studies at Bad Creek Reservoir, South Carolina. Final
662 Tech. Rep., U.S. Geol. Surv., Reston, Va, 89 p.
663
664 Van der Weijden, C.H., Pacheco, F.A.L., 2006. Hydrogeochemistry in the Vouga River basin (central
665 Portugal): pollution and chemical weathering. Appl. Geochem. 21, 580–613.
666 doi:10.1016/j.apgeochem.2005.12.006.

667 Verweij, J.M., 1995. Analysis of Pumping Test Data from Hard Rock Aquifers. TNO Report, Institute
668 of Applied Geoscience, England, v. GG R-95-39(A), 65 p.
669
670 White, A.F., Brantley, S.L., 2003. The effect of time on the weathering of silicate minerals: why do
671 weathering rates differ in the laboratory and field? Chem. Geol. 202, 479–506.
672 doi:10.1016/j.chemgeo.2003.03.001.
673
674 Wright, E.P., Burgess, W.D. (1992). The Hydrology of Crystalline Basement Aquifers in Africa.
675 Special Publication 66, Geological Society, London. 264 p. doi: 10.1144/GSL.SP.1992.066.01.01.

Figure 1

Click here to download high resolution image

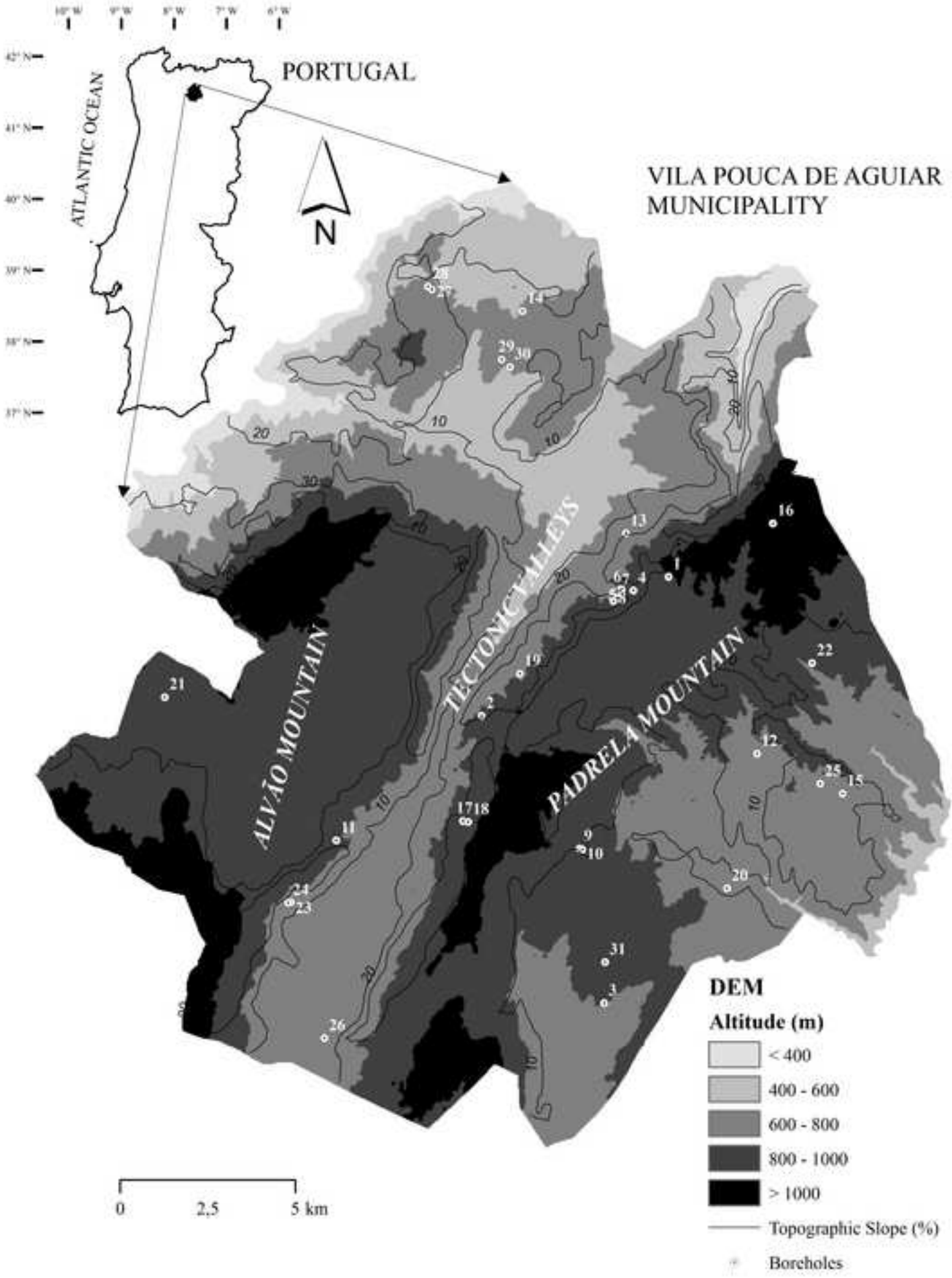

Figure 2

Click here to download high resolution image

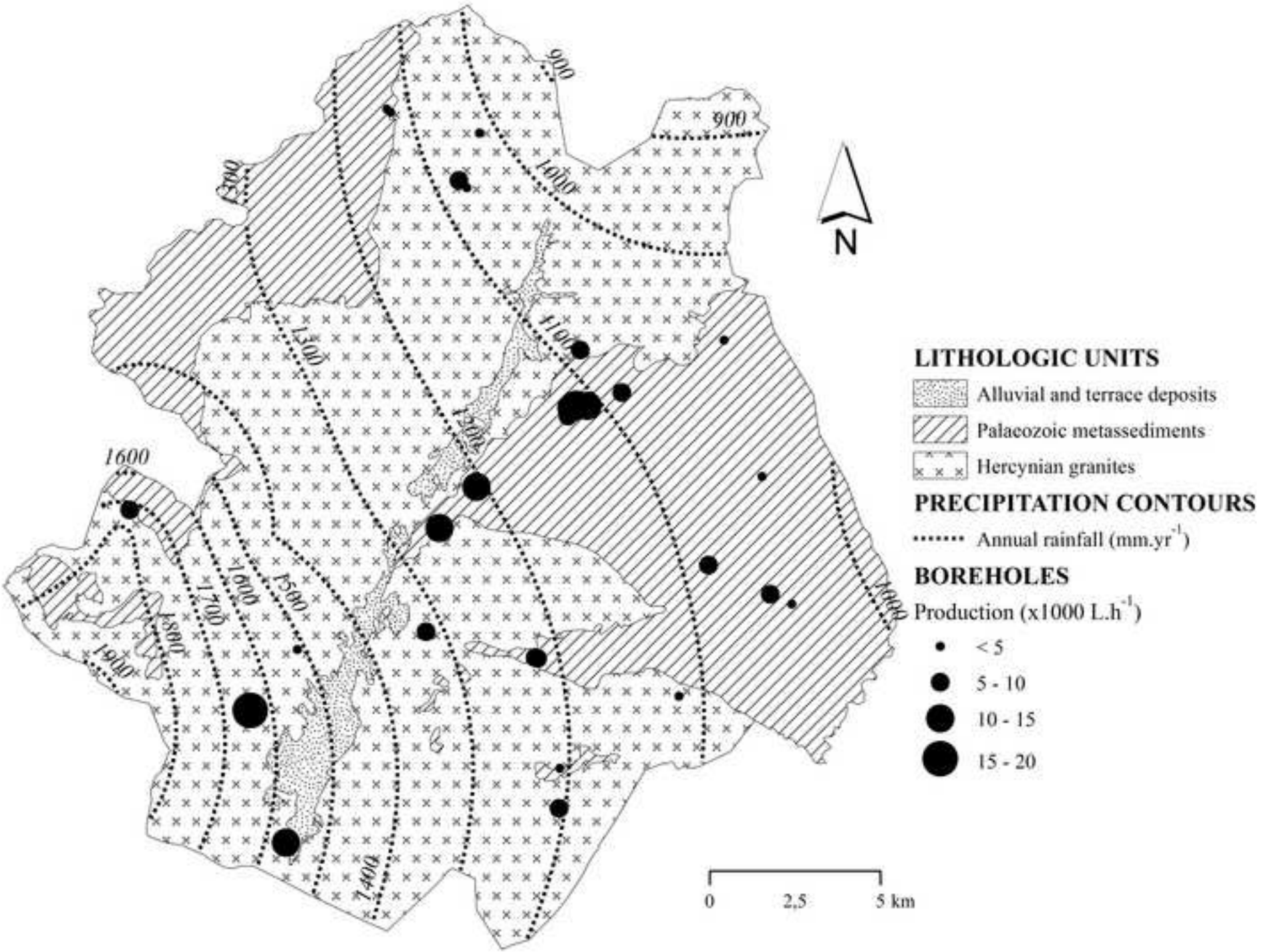

Figure 3

Click here to download high resolution image

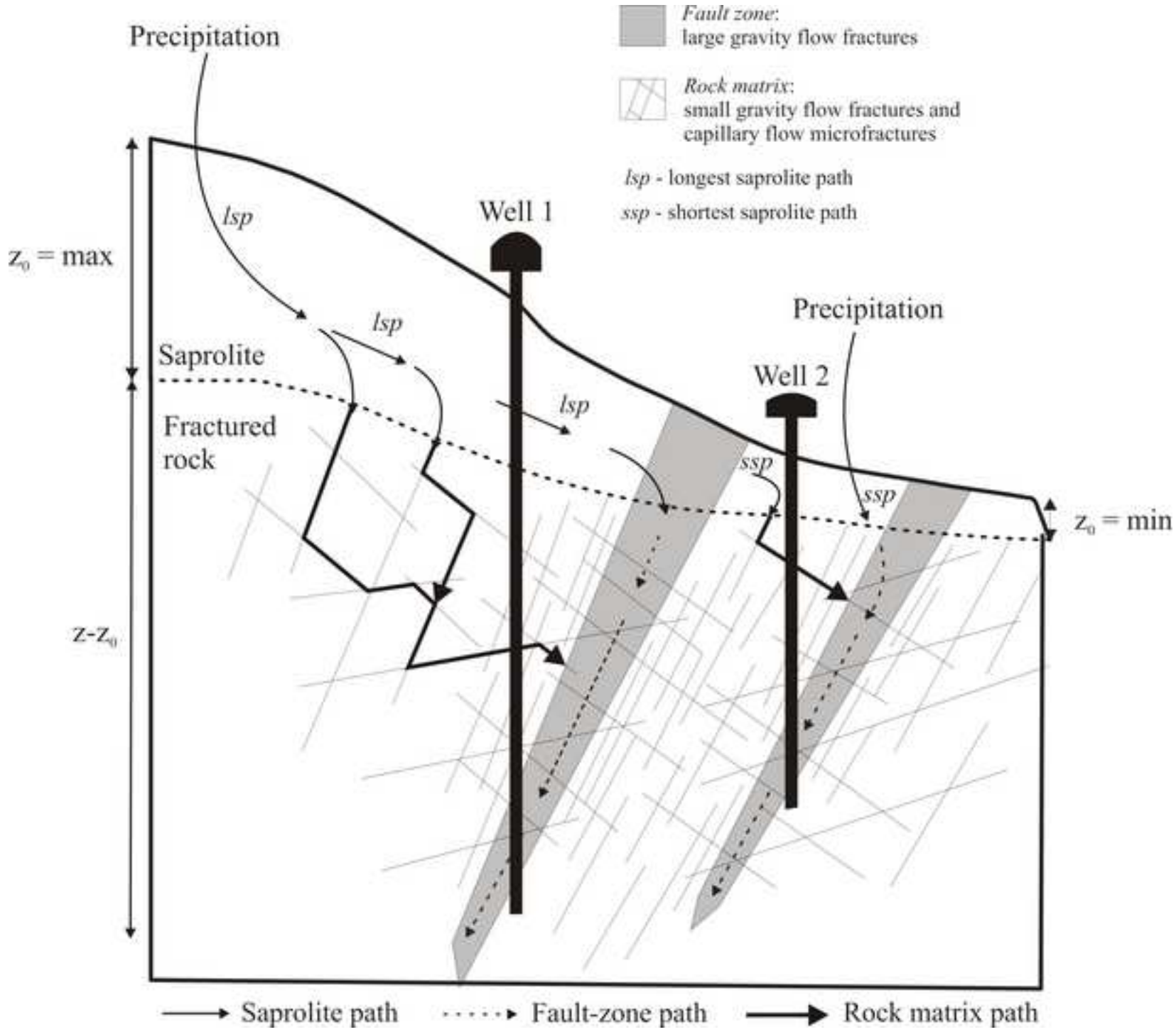

Figure 4

Click here to download high resolution image

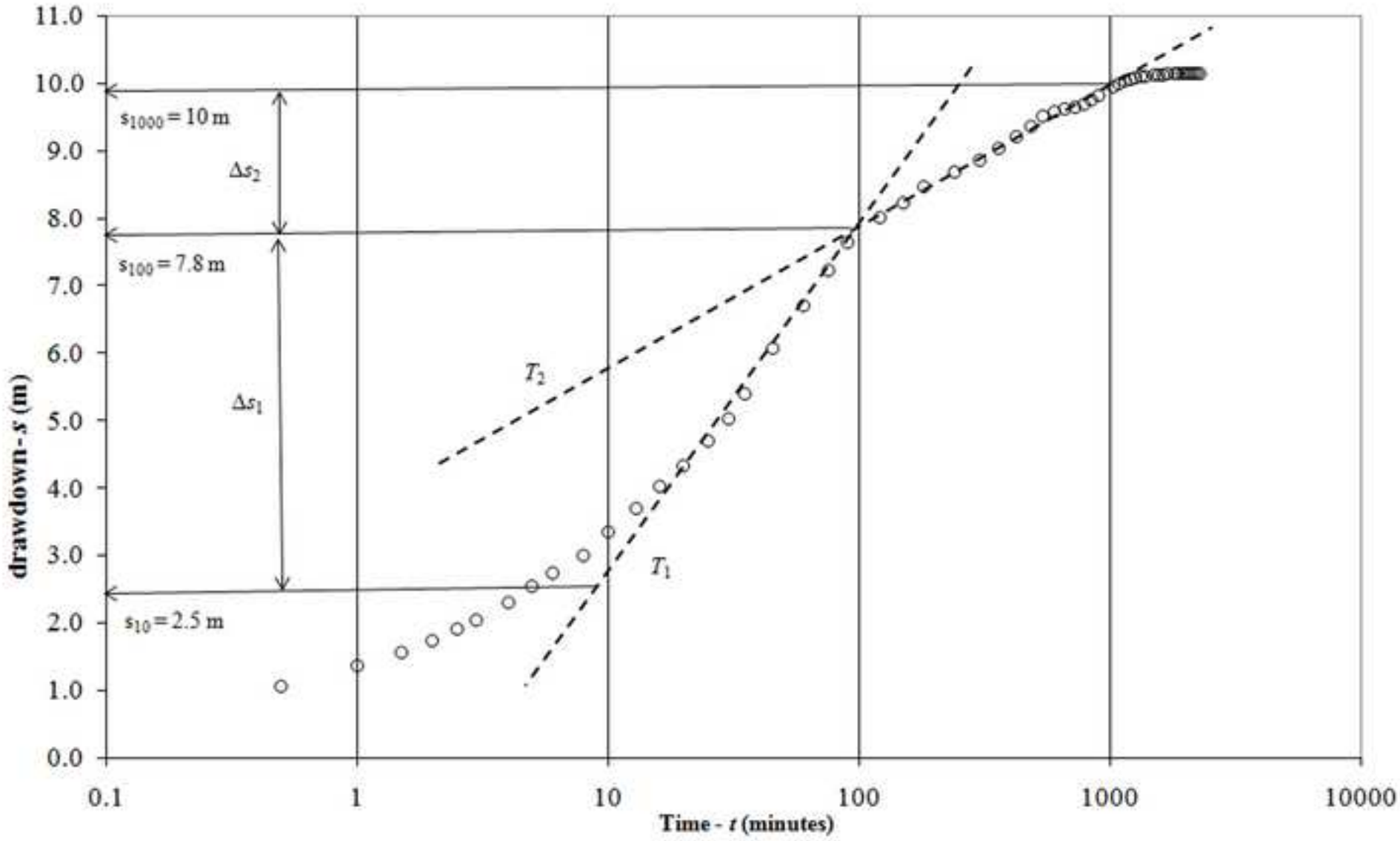

Figure 5

Click here to download high resolution image

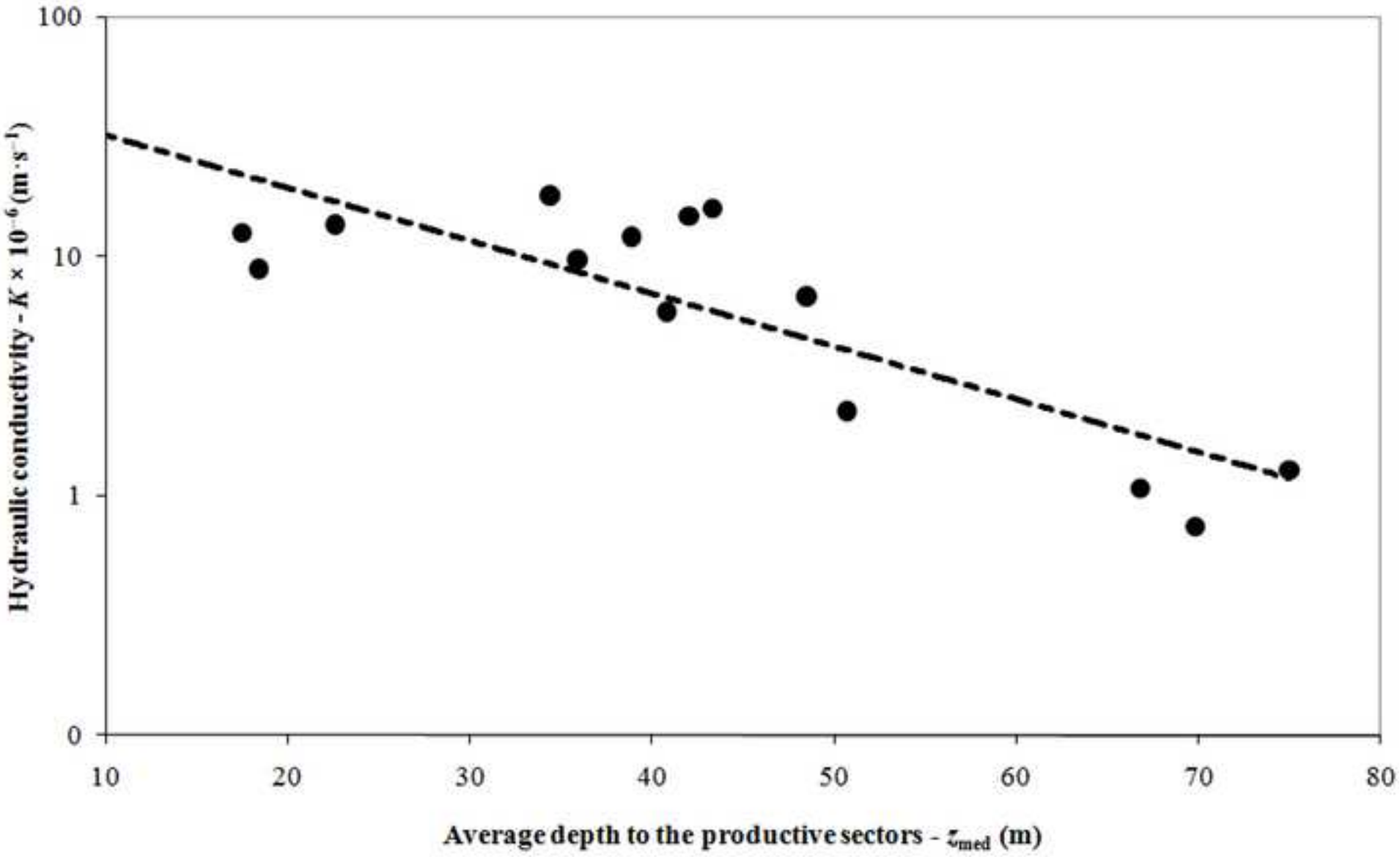

Figure 6

Click here to download high resolution image

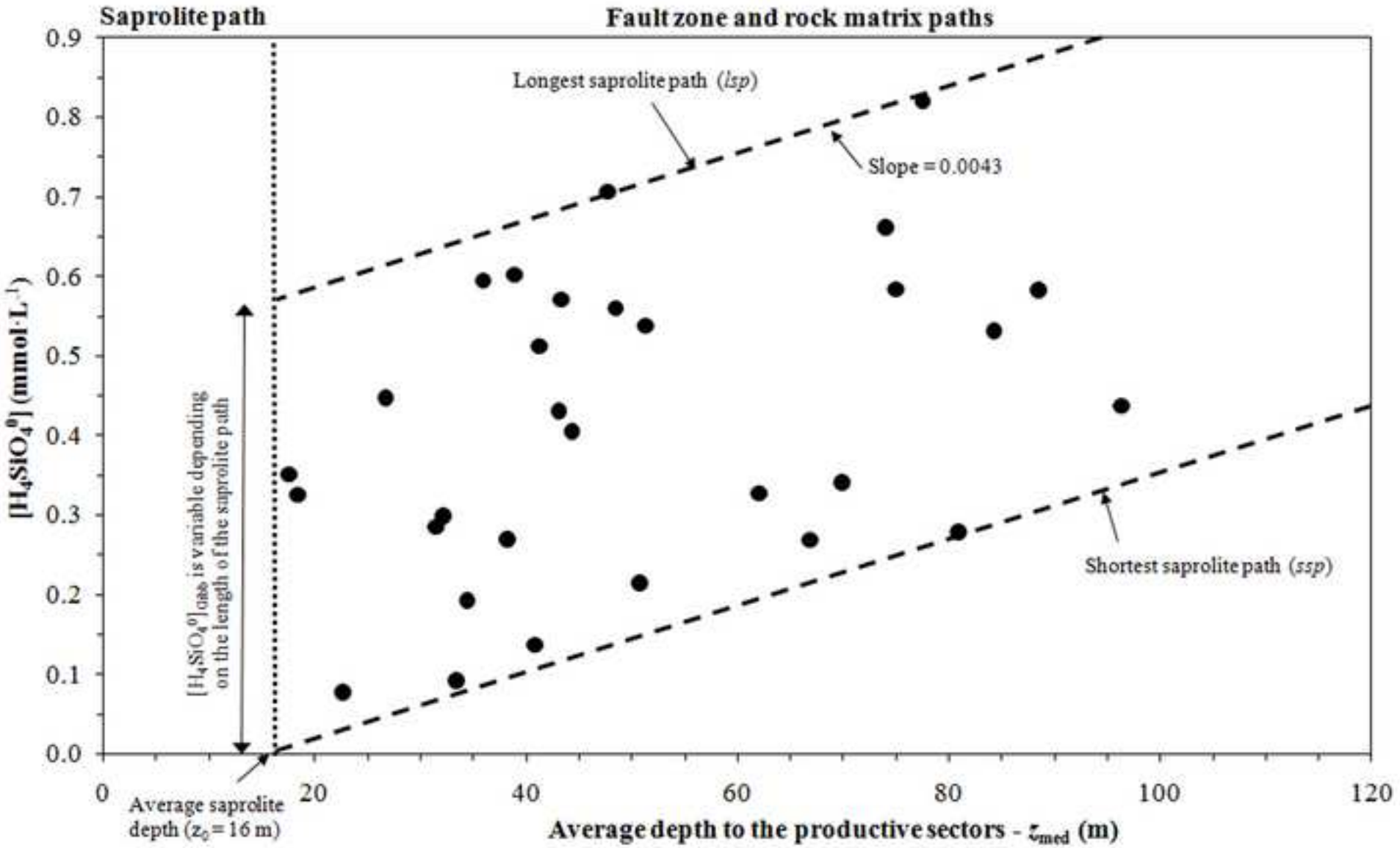

Figure 7

Click here to download high resolution image

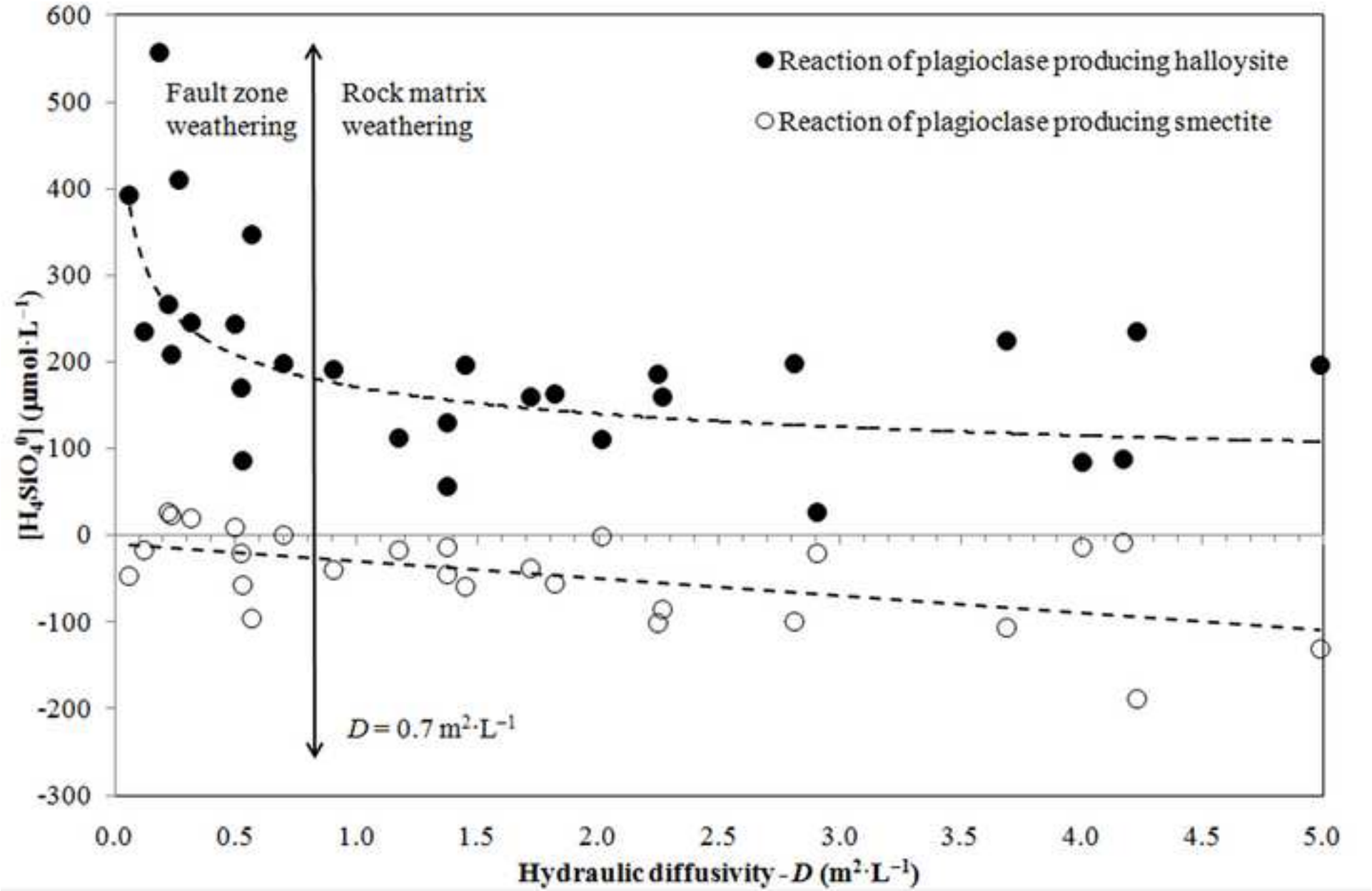

Figure 8

Click here to download high resolution image

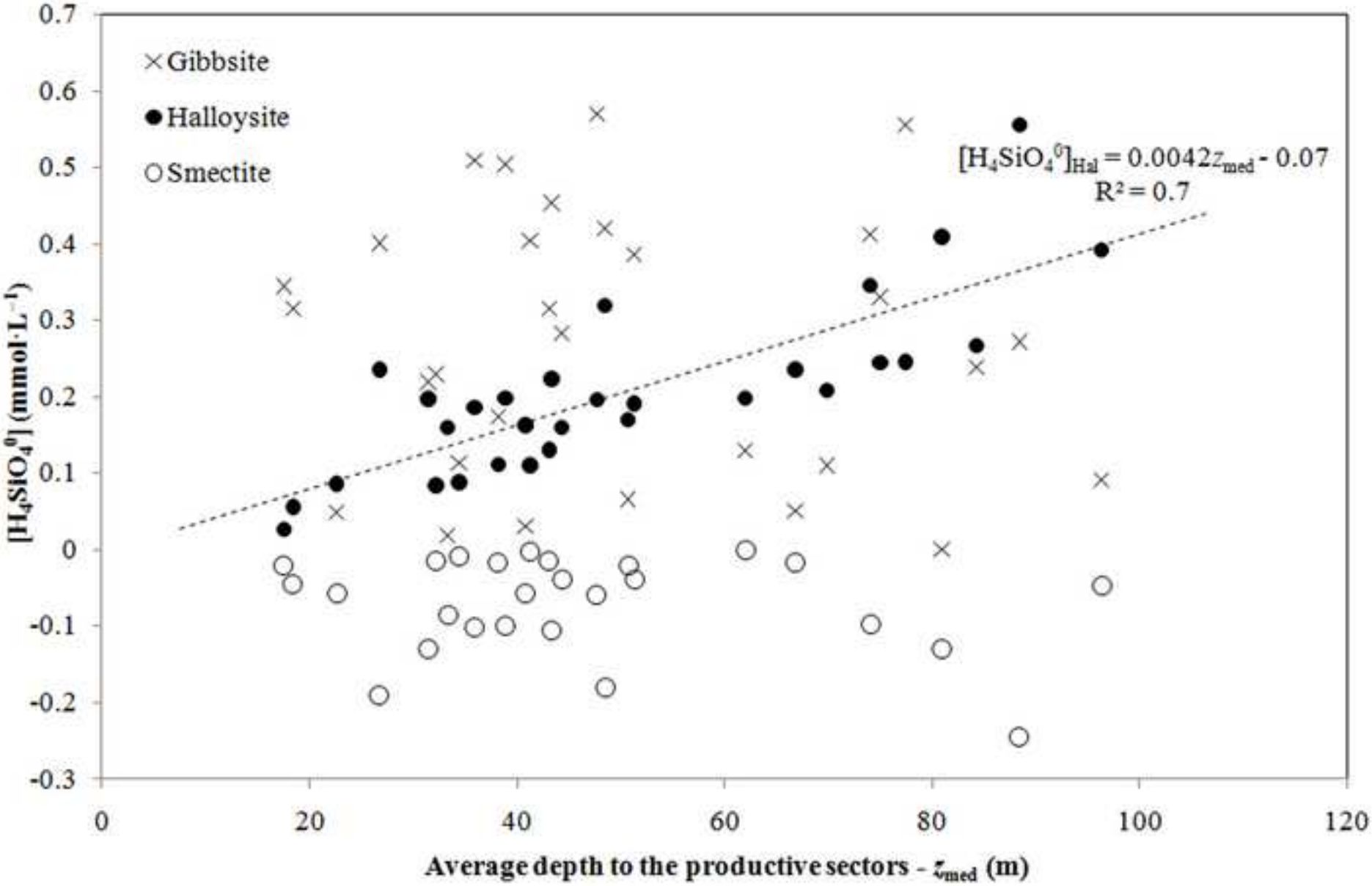

Figure 9

Click here to download high resolution image

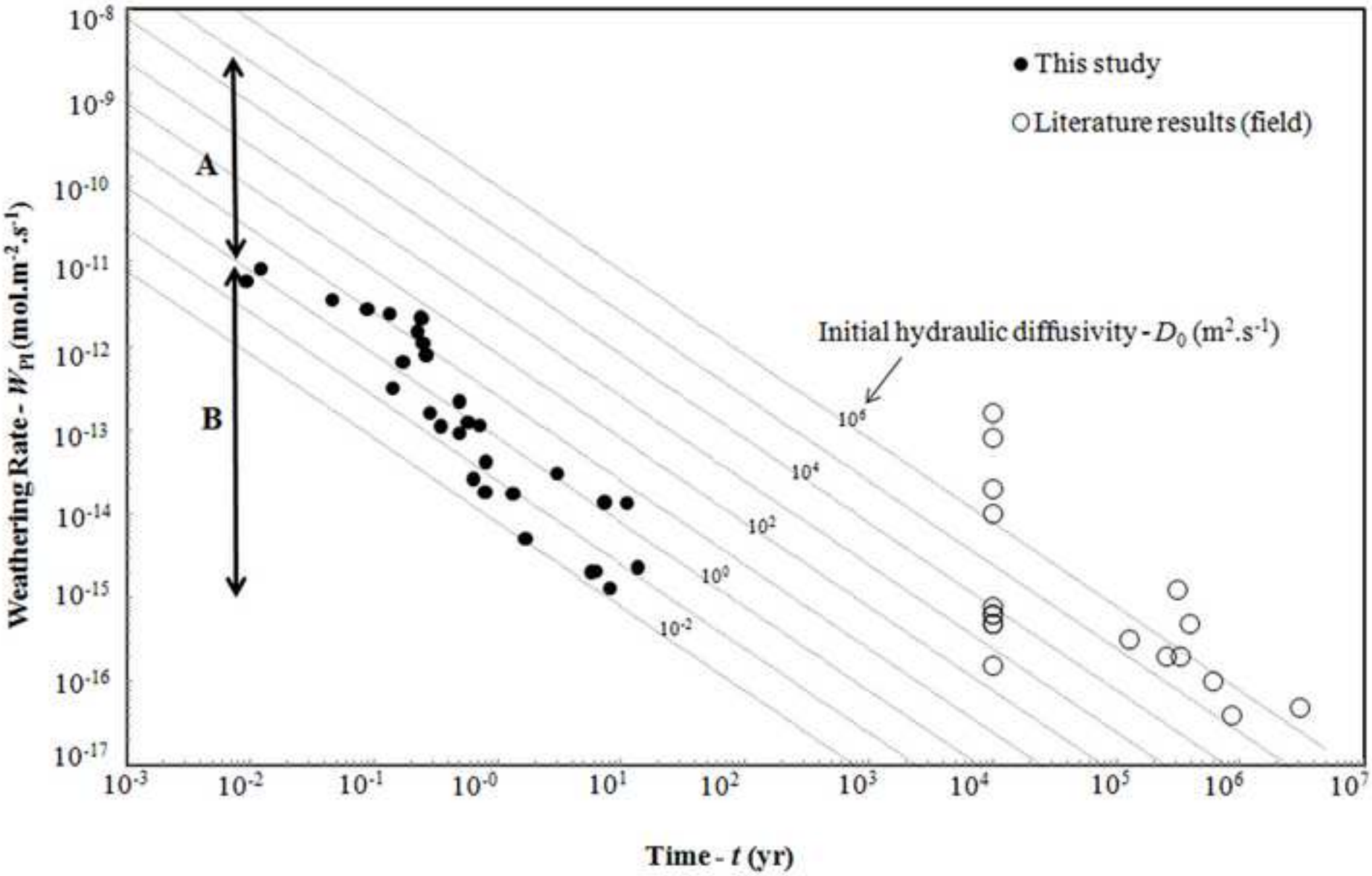

TABLE LEGENDS

Table 1 – Identification (Nr, Id), intersected rock type (A = granites; B = metassediments), and depth (z) of 31 boreholes drilled in the region of Vila Pouca de Aguiar. Slope (d) of the topographic surface around the borehole and precipitation (P) falling in its vicinity in one year. Depths (z_i, z_{med}) and water yields (Q_i, ΣQ) of fractures intersected during the execution of the drillings. The value of z_{med} is calculated by Equation 1.

Table 2 – Results of the hydraulic tests. Symbols: Nr – borehole identification, z_{med} – average depth to the productive sectors (Equation 1), b – drained thickness, t – pumping test duration, Q – pumping test discharge rate, h_0 – initial hydraulic head, s_t – drawdown at time t (10, 100 and 1000 minutes), Δs_t – change in drawdown corresponding to the log cycle of time t (10 to 100 and 100 to 1000 minutes), K_{med} – average hydraulic conductivity. (*) three meter long screened tubes, (**) one meter long screened tubes.

Table 3 – In *situ* hydraulic diffusivities of rocks and regoliths. References: 1 – Domenico and Schwartz (1998), 2 – Roeloffs (1997); 3 – Abrisqueta et al. (2006). Diffusivities of unweathered rocks are based on values of hydraulic conductivity and effective porosity reported in reference 1, and were estimated using Equations 3–5. Minimum and maximum regolith diffusivities were measured at water contents of 15% and 30%, respectively.

Table 4 – Hydrologic parameters of the sampled boreholes: hydraulic diffusivity (D; Equation 3), hydraulic conductivity (K; calculated by Equation 4 for the tested boreholes and estimated by Equation 15 for the non tested boreholes), drained thickness (b), and groundwater travel time (t; Equation 14). Results of the field and laboratory measurements:

electrical conductivity (*Ec*), temperature (*T*), pH, and measured bicarbonate ($[HCO_3^-]$) and silica ($[H_4SiO_4^0]$) concentrations of the borehole waters. Results of the weathering modelling: concentration of silica derived from plagioclase reactions R_{Gibb}, R_{Hal} and R_{Sm}, as depicted in Table 5 ($[H_4SiO_4^0]_{Gibb}$, $[H_4SiO_4^0]_{Hal}$ and $[H_4SiO_4^0]_{Sm}$); moles of plagioclase dissolved along the saprolite ($[Pl]_0$) and saprolite + fault zone + rock matrix ([Pl]) flow paths (Equation 8), and plagioclase weathering rates along the fault zone + rock matrix path (W_{Pl}; Equation 12b).

Table 5 – Reactions of plagioclase ($Na_{1-x}Ca_xAl_{1+x}Si_{3-x}O_8$, where *x* is the anorthite content) producing smectite ($(Mg_{0.35}Al_{1.65})Si_4O_{10}(OH)_2 \cdot 5H_2O \cdot Ca_{0.175}^{2+}$), halloysite ($Al_2Si_2O_5(OH)_4$) and gibbsite ($Al(OH)_3$). Structural formula of smectite adopted from Van der Weijden and Pacheco (2006).

TABLE 1

Nr	Id	Rock Type	z	d	P	z_1	z_2	z_3	z_4	z_5	z_6	z_{med}	Q_1	Q_2	Q_3	Q_4	Q_5	Q_6	ΣQ
			m	%	$mm \cdot y^{-1}$	m							$m^3 \cdot h^{-1}$						
1	Balugas	B	121	23.7	1087	85	97					96	0.5	8.5					9
2	Barreiros 2	B	101	40.5	1252	36	48	60	84			62	1.5	3.0	3.5	4.0			12
3	Barrela	A	83	9.6	1206	15	33	42	69			41	2.0	0.5	1.5	2.0			6
4	Bornes 1	B	90	19.6	1107	15	32	47				39	1.0	6.0	8.0				15
5	Bornes 2	B	83	41.7	1113	19	33	39				36	0.5	3.5	6.0				10
6	Bornes 3	B	74	32.6	1113	26	46	56				43	3.5	8.5	3.0				15
7	Bornes 4	B	80	33.1	1114	22	29	40	48			42	0.5	1.5	6.0	7.0			15
8	Bornes 5	B	92	46.0	1121	27	45	52				48	0.5	3.0	6.0				10
9	Campo de Jales 1	B	91	21.8	1221	27	43	57	70			48	0.5	4.5	1.0	1.0			7
10	Campo de Jales 2	B	130	24.7	1219	29	33	57	79	90	120	74	0.5	0.5	1.4	1.0	1.0	1.0	5
11	Castelo	A	122	33.5	1514	16	27	58	106			70	0.5	0.5	0.5	1.5			3
12	Covas	B	100	12.7	1084	51	63	68	84	92		75	1.0	1.0	1.0	1.0	2.0		6
13	Eiriz	A	110	17.7	1086	56	84	90	96			88	0.5	1.0	3.5	2.0			7
14	Freixeda	A	106	11.3	1022	15	19	60	72			44	0.2	0.5	0.3	0.5			2
15	Granja	B	90	16.9	1043	37	52	70				51	1.5	1.0	1.0				4
16	Lagoa	B	70	10.6	1041	25	30	45				33	1.0	1.0	1.0				3
17	Montenegrelo 1	A	151	18.4	1325	43	90	103	133			84	0.9	0.6	0.5	0.5			3
18	Montenegrelo 2	A	80	20.6	1320	30	47	62				43	2.5	3.5	1.0				7
19	Nuzedo	B	33	14.9	1206	13	22					18	6.0	9.0					15
20	Reboredo Novo	A	80	22.3	1115	13	27	49				34	0.5	2.5	2.0				5
21	Santa Marta	B	92	13.5	1727	14	18	37				23	2.0	2.5	2.0				7
22	Cevivas	B	88	34.3	1044	50	59	76				67	0.3	1.7	2.0				4
23	Souto	A	100	8.7	1637	18	22	30	40	60		32	2.0	1.0	0.5	1.5	1.0		6
24	Telões	A	121	17.0	1643	20	23	26	33	38	40	31	4.0	1.0	2.0	3.0	4.0	4.0	18
25	Treminas	B	112	16.4	1053	34	42	96	102			81	1.5	1.0	1.1	4.4			8
26	Vila Chã	A	91	16.5	1565	70	73	79	82			78	2.0	2.0	4.0	4.0			12
27	Vilaribho 1	B	85	24.7	1126	19	38	76				51	0.3	0.2	0.5				1
28	Vilarinho 2	B	95	34.2	1131	31	38	44	60			41	2.0	1.0	1.0	1.0			5
29	Vilela 1	A	91	5.1	1071	14	17	20	34			27	1.0	1.0	1.0	4.0			7
30	Vilela 2	A	110	11.7	1067	7	10	61				18	1.0	1.5	0.5				3
31	Vreia de Jales	B	121	9.3	1208	19	43					38	0.3	1.2					2

TABLE 2

Nr	z_{med}	b	t	$Q \times 10^{-3}$	h_0	s_{10}	s_{100}	s_{1000}	Δs_1	Δs_2	$K_{med} \times 10^{-6}$
	m	m	min	$m^3 \cdot h^{-1}$	m	m	m	m	m	m	$m \cdot s^{-1}$
4	39	18	2280	13.5	0.7	2.5	7.8	10.0	5.3	2.3	43.60
5	36	18	1620	10.8	9.7		1.4	4.6		3.2	34.88
6	43	18	1620	13.5	10.4		5.0	7.4		2.4	57.23
7	42	24	1980	13.5	15.1		1.0	2.9		2.0	52.82
8	48	18	1140	13.5	3.1		6.2	11.8		5.6	24.53
11	70	24	2640	3.0	9.5		25.5	34		8.5	2.69
12	75	30	1200	7.6	26.7		23.5	33.5		10.0	4.64
15	51	18	2760	3.6	18.5		4.5	9.0		4.5	8.14
19	18	12	1680	10.8	0.0	1.75	5.8	13.0	4.0	7.3	31.97
20	34	18	1440	5.4	0.0	1.7	2.6		0.9		64.63
21	23	3	2640	6.8	1.5		0.0	8.4		8.4	49.05
22	67	9	330	7.2	28.9		21.0	59.0		38.0	3.86
28	41	24	1920	5.0	18.7		5.1	6.9		1.8	21.19
30	18	18	1500	3.1	1.5		3.1	3.8		0.7	45.05

TABLE 3

Material	Hydraulic Diffusivity – D ($m^2 \cdot s^{-1}$)		Reference
	Minimum	Maximum	
Unweathered fractured crystalline rock (protolith)	3.41×10^{3}	6.39×10^{5}	1
Weathered fractured crystalline rock	1.00×10^{-1}	1.00×10^{1}	2
Regolith	2.90×10^{-9}	2.20×10^{-5}	3

TABLE 4

Nr	D	$K\times10^{-6}$	b	t	Ec	T	pH	$[HCO_3^-]$	$[H_4SiO_4^0]$	$[H_4SiO_4^0]_{Gibb}$	$[H_4SiO_4^0]_{Hal}$	$[H_4SiO_4^0]_{Sm}$	$[Pl]_0$	[Pl]	$W_{Pl}\times10^{-13}$
	$m^2\cdot s^{-1}$	$m\cdot s^{-1}$	m	yr	$\mu S\cdot cm^{-1}$	ºC		$\mu mol\cdot L^{-1}$							$mol\cdot m^{-2}\cdot s^{-1}$
1	0.06	0.4	12	13.70	106	7.4	6.5	520	437	92	392	-47	33	705	0.02
2	0.70	2.3	24	0.80	38	11.8	5.8	207	328	130	198	-1	46	175	0.18
3	2.02	6.5	24	0.64	69	13	6.0	264	513	404	111	-2	144	231	0.26
4	2.81	12.1	18	0.25	130	14.3	6.8	766	602	504	199	-100	180	1222	10.83
5	2.25	9.7	18	0.09	129	13.8	6.7	761	595	509	186	-101	182	1221	27.46
6	3.69	15.9	18	0.23	120	12.8	6.8	787	571	454	224	-106	162	1275	14.67
8	3.41	14.7	18	0.25	151	13	6.9	1141	560	421	320	-180	150	2002	21.43
9	1.45	4.7	24	0.49	87	11.4	6.4	628	707	570	196	-59	204	868	2.19
10	0.57	1.2	36	3.05	112	13.3	6.8	823	662	412	346	-97	147	1250	0.30
11	0.23	0.7	24	1.68	157	12.2	5.6	113	342	110	209	nd	39	170	0.05
12	0.50	1.3	30	6.30	112	11.8	6.0	287	584	331	244	nd	118	271	0.02
13	0.18	0.6	24	11.06	236	6.9	7.4	1513	584	272	556	-245	97	2689	0.13
14	1.72	5.6	24	0.71	62	13.4	5.9	395	405	283	160	-38	101	553	1.12
15	0.53	2.3	18	0.81	38	13.9	5.7	239	215	66	170	-21	24	321	0.41
16	2.26	9.8	18	0.27	38	12.2	6.3	469	93	18	160	-85	6	888	7.79
17	0.22	0.7	24	8.12	47	11.2	6.0	195	532	239	267	nd	85	252	0.01
18	1.38	5.9	18	0.35	39	11.2	5.9	290	432	315	131	-14	113	325	1.11
19	1.37	8.9	12	0.01	57	12.2	6.2	361	326	315	56	-46	113	568	83.08
20	4.17	18.0	18	0.14	33	12.9	5.4	151	193	114	88	-9	41	178	3.09
21	0.53	13.6	3	0.05	51	12.2	5.9	316	77	49	86	-58	17	600	34.89
22	0.12	1.1	9	1.33	56	12.9	5.9	266	269	50	235	-17	18	320	0.18
23	4.01	10.3	30	0.28	41	12.9	5.8	220	299	230	84	-15	82	268	1.58
24	4.99	10.7	36	0.13	66	13.2	6.6	764	286	219	197	-131	78	1398	24.23
25	0.27	0.9	24	7.29	100	10.8	6.8	830	279	0	409	-131	0	1453	0.14
26	0.32	1.0	24	5.76	78	15.4	6.1	348	820	556	246	nd	198	352	0.02
27	0.91	3.9	18	0.58	66	14.4	6.2	466	538	386	191	-39	138	617	1.22
28	1.82	5.9	24	0.17	52	12.1	5.9	361	137	31	163	-56	11	629	6.52
29	4.23	13.7	24	0.24	256	14.8	7.0	1107	447	401	236	-189	143	2027	21.64
30	2.91	12.5	18	0.01	114	13.9	6.0	251	351	345	27	-21	123	330	58.98
31	1.18	7.6	12	0.50	42	4.8	5.8	225	270	174	112	-16	62	283	0.92

TABLE 5

Id	Clay Mineral	Reaction
R_{Gibb}	gibbsite	$\frac{2}{1+x}\mathrm{Pl} + 2\mathrm{CO_2} \xrightarrow{n\mathrm{H_2O}} \mathrm{Gb} + 2\frac{1-x}{1+x}\mathrm{Na^+} + 2\frac{x}{1+x}\mathrm{Ca^{2+}} + 2\mathrm{HCO_3^-} + 2\frac{3-x}{1+x}\mathrm{H_4SiO_4^0}$
R_{Hal}	halloysite	$\frac{2}{1+x}\mathrm{Pl} + 2\mathrm{CO_2} \xrightarrow{n\mathrm{H_2O}} \mathrm{Hal} + 2\frac{1-x}{1+x}\mathrm{Na^+} + 2\frac{x}{1+x}\mathrm{Ca^{2+}} + 2\mathrm{HCO_3^-} + 4\frac{1-x}{1+x}\mathrm{H_4SiO_4^0}$
R_{Sm}	smectite	$\frac{1.65}{1+x}\mathrm{Pl} + 0.35\mathrm{Mg^{2+}} + 0.6\mathrm{CO_2} \xrightarrow{n\mathrm{H_2O}}$ $\mathrm{Sm} + 1.65\frac{1-x}{1+x}\mathrm{Na^+} + \frac{1.475x - 0.175}{1+x}\mathrm{Ca^{2+}} + 0.6\mathrm{HCO_3^-} + \frac{0.95-5.65x}{1+x}\mathrm{H_4SiO_4^0}$

FIGURE CAPTIONS

Figure 1 – Location and Digital Elevation Model (DEM) of the Vila Pouca de Aguiar region. Distribution of topographic slopes (contour lines) and of studied drilled wells (filled circles). The numbers close to the circles are in agreement with the numbers under the heading "Nr" in Tables 1, 2 and 4.

Figure 2 – Simplified geologic map of the Vila Pouca de Aguiar region. Spatial distribution of annual precipitation (contour lines) and production of drilled wells used for public supply of drinking water (graduated filled circles).

Figure 3 – Flow paths of shallow groundwater towards and within fault zones. Characteristic fractures prevailing in fault zone and rock matrix environments. Weathering of plagioclase along the saprolite path is described by R_{Gibb} (Table 5) producing $[H_4SiO_4^0]_{Gibb}$, along the fault zone path by R_{Hal} producing $[H_4SiO_4^0]_{Hal}$, and along the rock matrix path by R_{Sm} and R_{Hal} producing $[H_4SiO_4^0]_{Sm}$ and $[H_4SiO_4^0]_{Hal}$. When the saprolite path is the shortest (ssp), it is assumed that $[H_4SiO_4^0]_{Gibb} = 0$, when is the largest (lsp) that $[H_4SiO_4^0]_{Gibb} = \max$.

Figure 4 – Semilogarithmic plot of drawdown (*s*) *versus* time (*t*) relative to borehole Bornes 1 (Nr = 4). The description of symbols and interpretation of the graph is given in the text.

Figure 5 – Relation between hydraulic conductivity (*K*) and average depth to the productive sectors of the drilled wells (z_{med}).

Figure 6 – Relation between concentration of dissolved silica ($[H_4SiO_4^0]$) and depth to the productive sectors of the drilled wells (z_{med}). The lower and upper dashed lines describe the evolution of dissolved silica concentrations along the fault zone plus rock matrix paths when the saprolite path has been the shortest (*ssp*, see also Figure 3) or the longest (*lsp*), respectively. Regardless of the saprolite path, dissolved silica concentrations increase 0.0043 $mmol \cdot L^{-1}$ per unit depth. The *ssp* line intersects the *x*-axis where z_{med} = 16 m (z_0). Making a note that the *ssp* corresponds to vertical flow of groundwater towards the fault zone (Figure 3), z_0 represents the average thickness of the saprolite layer. The concentration of dissolved silica at the beginning of the fault zone plus rock matrix paths, in cases where the saprolite path is *lsp*, is marked by the intersection between the upper dashed and the dotted line.

Figure 7 – Relation between concentration of dissolved silica ($[H_4SiO_4^0]$) and hydraulic diffusivity (*D*). $D \approx 0.7\ m^{-2} \cdot s^{-1}$ is the threshold assumed to separate fault zone (open system) weathering, where the prevailing reaction is R_{Hal} (Table 5), from rock matrix (semi-open system) weathering where R_{Hal} as well as R_{Sm} play a role in plagioclase weathering.

Figure 8 – Relation between depth to the productive sectors of the drilled wells (z_{med}) and concentration of dissolved silica ($[H_4SiO_4^0]$), discriminating the weathering reactions

involved (R_{Sm}, R_{Hal} and R_{Gibb}; Table 5). Only the concentrations related to R_{Hal} correlate with z_{med}, meaning that only halloysite represents weathering of plagioclase along advective flow paths (gravity fractures of the fault zones and rock matrix).

Figure 9 – Plot of weathering rates *versus* time. The filled circles represent present study rates, the open circles literature results compiled from White and Brantley (2003). The dotted lines are graphical representations of Equation 17, for various initial hydraulic diffusivities (D_0). The double arrowed lines represent the role of hydraulic diffusivity change (line A) and time (line B) in the drop off of weathering rates, relative to the presumed rate of an average protolith (unweathered rock).